12-2017

Sulfur Isotope Variations in the Elk Creek Carbonatite Complex, Southeastern Nebraska, USA

Emily Campbell
University of Nebraska-Lincoln, emily.campbell26@gmail.com

Sulfur Isotope Variations in the Elk Creek Carbonatite Complex, Southeastern Nebraska, USA

by

Emily Madeliene Campbell

A THESIS

Presented to the Faculty of

The Graduate College at the University of Nebraska

In Partial Fulfillment of Requirements

For the Degree of Master of Science

Major: Earth and Atmospheric Sciences

Under the supervision of Professor Richard M. Kettler

Lincoln, Nebraska

December, 2017

SULFUR ISOTOPE VARIATIONS IN THE ELK CREEK CARBONATITE COMPLEX, SOUTHEASTERN NEBRASKA, USA

Emily Madeliene Campbell, M.S.

University of Nebraska, 2017

Advisor: Richard M. Kettler

The Elk Creek Carbonatite Complex (ECCC) comprises eight different units of carbonatite and silicate rocks, including a magnetite-dolomite carbonatite that hosts the largest niobium deposit in the United States. This study focused on interpreting the first set of sulfur isotopes from this system to decipher between magmatic and secondary processes. Using sulfur isotope variations I was able to discriminate between hypogene and supergene mineralization, and measure (1) formation temperatures (2) possible sulfur source (3) degassing effects on isotopic composition, and (4) post-magmatic alteration. The groundwork for mapping and interpreting iron oxide alteration is also laid out in this thesis.

Hypogene mineralization displays isotopic fractionation between sulfate and sulfide minerals similar to other carbonatites worldwide. The $\delta^{34}S$ values for primary mineralization range from +1.77‰ to +11.06‰ for sulfates and -10.85‰ to +2.31‰ for sulfides. Sulfide-sulfate mineral pairs yielded equilibrium formation temperatures ranging from 660°C to 730°C. In addition to temperature, $\delta^{34}S$ values for bulk sulfur ($\delta^{34}S_{\Sigma S}$) were determined. The calculated range for $\delta^{34}S_{\Sigma S}$ is -2.23‰ to -1.64‰, which is representative of a mantle source.

Degassing during magma evolution altered sulfide-sulfur isotope composition. As a result of H_2S outgassing, several pyrite samples were enriched in ^{34}S having $\delta^{34}S$ values of +0.6‰, +2.26‰, and +2.31‰. These values are more enriched in ^{34}S compared to hypogene sulfide.

Supergene sulfate has $\delta^{34}S$ values ranging from -11.89‰ to -4.31‰. These values are significantly depleted compared to hypogene sulfates. In addition to $\delta^{34}S$ values, $^{87}Sr/^{86}Sr$ values were used as evidence that supergene alteration occurred. Three anomalously high $^{87}Sr/^{86}Sr$ values have values similar to Pennsylvanian seawater and sedimentary rocks.

Iron oxide alteration is prevalent in the ECCC, and could be a potential issue for future mining projects. Thick iron oxide veins could be a serious problem for the stability of an underground mine. When altered, by hematite or limonite, the carbonatite rock becomes friable and brittle. Identifying and mapping these veins would be of utmost importance to mine construction.

DEDICATION: I would like to dedicate this work to my grandparents, Peter and Margaret Campbell and Lou and Madeleine Prost, for giving me the blood of a miner and the means to pursue my degree.

ACKNOWLEDGEMENTS: I would like to first thank my advisor, Dr. Richard Kettler for all his support and encouragement. I would also like to thank my committee members, Dr. R.M. Joeckel and Dr. Lynne Elkins for their invaluable input during thesis revisions. Also, I would like to give a big thanks to the Conservation and Survey Division of the University of Nebraska-Lincoln for permission to sample core from the Mead, Nebraska core repository and access to ancillary data.

Thank you to Dr. Robert Seal of the USGS in Reston, Virginia. Without the help of him and his lab, I would not have had the tools necessary to obtain my data. Thank you to Niocorp Developments and Dahrouge Geological Consulting for allowing me to collect samples during the Phase II and III exploration project in 2014.

Finally I would like to thank my family, especially my parents John and Colette Campbell, for all their love and encouragement through this process. A special thank you to Kasey Hurd for his love and support.

GRANT INFORMATION: Funding was provided from the Nebraska Geological Society's Yatkola-Edwards Award, and two semesters as a Graduate Research Assistant from the Department of Earth and Atmospheric Sciences.

TABLE OF CONTENTS

List of Figures

List of Tables

1. Introduction

In this thesis I report the first $\delta^{34}S$ values from the Elk Creek Carbonatite Complex (ECCC) and evaluate the mechanisms that control these values, including magma evolution, degassing, and post-magmatic supergene alteration. In addition to the $\delta^{34}S$ values, a second evaluation of $^{87}Sr/^{86}Sr$ values from previous work published by Brookins et al. (1975) will be conducted in this thesis to test the possibility that these ratios were affected by supergene alteration. Although detailed sulfur isotope studies are typically important in studies of ore genesis, the $\delta^{34}S$ values of carbonatites have received relatively little attention. Carbonatite petrogenesis has been highly debated since the rock type was discovered. Prior to development of a mantle origin hypothesis, a melted limestone hypothesis was explored (Heinrich, 1966). The melted limestone hypothesis has recently been re-examined by several authors (Lentz, 1999; Chen et al., 2016). If melted limestone developed into carbonatite magma, one might expect that the $\delta^{34}S$ values would represent a seawater origin (+7‰ to +40‰) (Seal et al., 2006; Planavsky et al., 2012). This thesis therefore, provides a test of the melted limestone hypothesis.

Sulfur- bearing minerals are abundant in carbonatites. There are, however, only a handful of published $\delta^{34}S$ data sets. Sulfide minerals found in carbonatites include pyrite, chalcopyrite, galena, arsenopyrite, pyrrhotite, pentlandite, bornite, cubanite, marcasite, millerite, molybdenite, and sphalerite (Farrell et al., 2010). Pyrite and chalcopyrite are the most widespread of this group. Sulfate minerals found in carbonatites include barite, gypsum, and jarosite (Farrell et al., 2010).

Measurements of $\delta^{34}S$ values have been used to assess the origin of sulfur in hydrothermal fluids (Ohmoto and Rye, 1979;Ohmoto and Goldhaber, 1997), and magmas (Nikiforov et al., 2006). They have been used to measure the temperature, oxygen fugacity and differentiation stage of magmas (Mitchell and Krouse, 1971; Drüppel et al., 2006; Gomide et al, 2013). Finally, $\delta^{34}S$ values have been used to identify specific mechanisms of mineralization and magmatic degassing (Ohmoto and Rye, 1979; Yongfei, 1990; Ohmoto and Goldhaber, 1997; Marini et al, 2011; Gomide et al., 2013). These efforts have included studies of carbonatite systems. Sulfur isotope data can also be used to evaluate whether sulfates are the product of hypogene processes or sulfide weathering (Field, 1966; Deines, 1989). Hypogene and supergene minerals are defined in this thesis as mineralization derived from ascending fluids and mineralization derived from descending fluids, respectively. For example, $\delta^{34}S$ values have been used to discern between hypogene and supergene origins of sulfur-bearing minerals in carbonatites from Central Tuva (a state of the Russian Federation) (Nikiforov et al., 2006).

This research contains the largest set of $\delta^{34}S$ values obtained from any single carbonatite system in the world. In total, 64 samples of sulfate and sulfide minerals from the ECCC were analyzed. The $\delta^{34}S$ values range from -11.89‰ to +16.67‰ and are interpreted to result from both magmatic and supergene processes. The majority of $\delta^{34}S$ values for sulfate minerals (barite) in the ECCC are unlike those reported for any other carbonatite system to date, and are evidence for deep supergene alteration.

A re-evaluation of the $^{87}Sr/^{86}Sr$ values reported by Brookins et al. (1975) are provided to support the supergene alteration hypothesis. Brookins et al. (1975) measured $^{87}Sr/^{86}Sr$ values, strontium concentration, and barium concentration of 18 whole-rock samples. Three of the 18 samples had significantly higher $^{87}Sr/^{86}Sr$ values than the rest. These elevated values are interpreted here as evidence of supergene alteration.

2. Elk Creek Carbonatite Complex Discovery and Exploration History

The Elk Creek Carbonatite Complex (ECCC) (Fig. 1) is located along the border between Johnson and Pawnee counties in Southeast Nebraska. It was discovered in 1970 during a geophysical framework program in southeastern

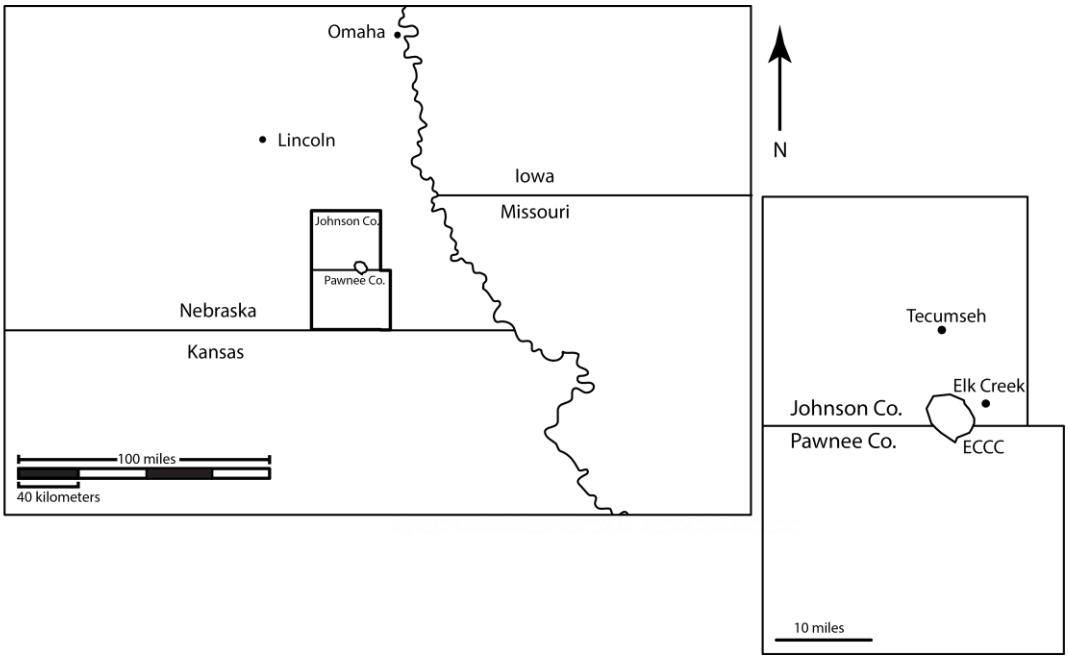

Fig. 1. Map showing the location of the study area in Southeast Nebraska. The Elk Creek Carbonatite (ECCC) is situated on the county line of Johnson and Pawnee counties.

Nebraska (Carlson and Treves, 2005) conducted by the Conservation and Survey Division (CSD) of the University of Nebraska- Lincoln. A near circular feature having gravity relief of 8 mgal and a magnetic anomaly of 800 gamma was identified and drilled (Carlson and Treves, 2005). The intrusion was eventually identified as a carbonatite based on core from test drill holes.

Initial geochronology was preformed by the United States Geological Survey (USGS) Isotope Laboratory using the K-Ar method on a sample of biotite from silicate rock. This biotite yielded an age of 544 ± 7 Ma (personal communications with Z.E. Peterman 1985, reported by Carlson and Treves, 2005). Two other biotite samples were dated, also using the K-Ar method, at Georgia State University, which yielded dates of 464 ± 5 and 484 ± 5 Ma (personal communications with M. Ghazi, reported by Carlson and Treves, 2005). More recently Farmer et al. (2013), conducted U/Pb analysis of zircons from syenite and obtained ages of 480 ± 20 and 540 ± 14 Ma. Sm-Nd isochrons from whole-rock analysis of the carbonatite agree with these ages (Farmer et al., 2013).

At 200 m subsurface the carbonatite is encountered. Molycorp drilled a total of 106 boreholes from 1977 to 1986. They collected over 24,000 m of core during this period (Carlson and Treves, 2005). The deepest drill hole was 1038 m subsurface, and bottomed out in carbonatite. The location of the drill holes sampled in this thesis is located in Appendix C (Fig. 1).

Quantum Rare Earth Developments (Quantum) acquired the rights to the ECCC in 2010. Quantum drilled 5 holes into the ECCC in 2011, totaling 3,419.85 m of

core. NioCorp Developments Ltd (NioCorp), previously known as Quantum Rare Earth Developments, again drilled the ECCC in a 2014 exploration project for a total of 15,482.8 m of core from 19 holes (SRK Consulting, 2015). Drilling by NioCorp in 2014 focused solely on the identified zone of niobium mineralization, while Molycorp drilled throughout the entire intrusive body.

3. Geologic Setting

The ECCC is located on the eastern flank of the 1.1 Ga Midcontinent Rift System (MRS). It is common for carbonatites to be associated spatially with intracontinental rift systems. However, the ECCC is significantly younger than the MRS by ~600 Ma. The MRS extends for more than 2,000 km, from Kansas to Lake Superior (Nicholson et al., 1996), cutting through southeastern Nebraska (Fig. 2). During the 25 million years of active rifting, voluminous amounts (approximately 2 X 10^6 km^3) of volcanic rocks were erupted (Cannon and Hinze, 1992). The deepest portion of the rift, estimated to be 30 km deep, is filled with ~20 km of volcanic rocks and ~10 km of sediment (Nicholson et al., 1996). The rift related volcanic rocks and sedimentary rocks are referred to as the Keweenawan Supergroup. Keweenawan volcanism was dominated by subaerial tholeiitic basalt flows with lesser intermediate and rhyolitic rocks (Nicholson et al., 1996).

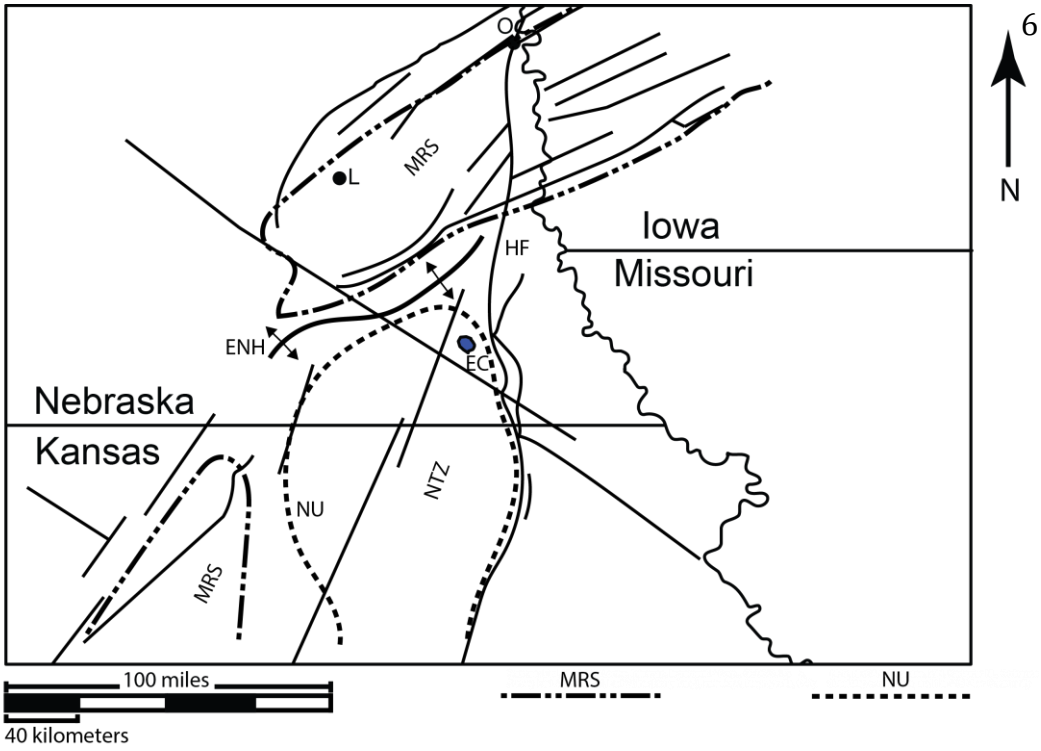

Fig. 2. Map location of various geologic features around the study area: Midcontinent Rift System (**MRS**), Nemaha Tectonic Zone (**NTZ**), Elk Creek Carbonatite Complex (**EC**), Humbolt Fault (**HF**), Eastern Nebraska High (**ENH)** schematic adapted from Burchett (1980), and the cities of Lincoln (**L**) and Omaha (**O**). The location of the MRS, NTZ, and all fault lines are adapted from Burberry et al. (2015). The dashed lines are schematic boundaries of the MRS adapted from Ojakangas et al. (2001), and the Nemaha Uplift (**NU**) adapted from Steeples et al. (1979).

The MRS cuts across Precambrian terranes of different ages, structure, and chemical composition (Van Schmus and Hinze, 1985). The Nebraska-Kansas segment of the rift formed in Proterozoic terranes, the Penokean Volcanic Belt and the Central Plains Orogenic Belt. The boundary of the two terranes has been mapped as the Humboldt Fault (Fig. 2) (Anderson, 1997).

The area surrounding the MRS in Nebraska comprises several geologic features. This area was mainly active from latest Proterozoic Eon to late Paleozoic Era. The area has undergone recent reactivation as evidenced by earthquakes (Burberry et al., 2015). The late Precambrian Eon (Neoproterozoic Era) feature in

Nebraska is the emplacement of the carbonatite, and early Paleozoic features are the Southeast Nebraska Arch and the Nemaha Uplift.

The ECCC sits upon the crest of the Nemaha Uplift. The Nemaha Uplift is a feature that was created approximately 300 Ma (Carlson and Treves, 2005). The Nemaha Uplift is a culmination of complex structural features, how ever in its simplest form, it is a gentle anticline folding over more pronounced basement highs (Dolton and Fin, 1989).

4. Lithology and Paragenesis

The ECCC is lithologically diverse containing eight different units of carbonatite and silicate rock. For a complete description of all eight units see Xu (1996) and Blessington (2014). The following descriptions of the rock types sampled, dolomite carbonatite, magnetite-dolomite carbonatite, and lamprophyre and mafic dikes, are based off observations over the duration of this research unless otherwise cited.

Table 1 provides the historic names used by Molycorp drill logs and previously published articles (Drenth, 2014), and the updated nomenclature used in Niocorp Developments drill logs and this research.

Table 1 Historic and present day nomenclature for the ECCC.

Historic	Present Day
Dolomite Beforsite	Dolomite Carbonatite
Magnetite Beforsite	Magnetite-Dolomite Carbonatite
Beforsite Breccia	Dolomite Carbonatite Breccia
Younger Mafic	Lamprophyre
Older Mafic	Mafic
Apatite Beforsite (I & II)	Apatite-Dolomite Carbonatite
Barite Beforsite	Barite-Dolomite Carbonatite
Syenite	Syenite

The apatite-dolomite carbonatite is a variant of the dolomite carbonatite (Table 1). Although Molycorp extensively mapped apatite-dolomite carbonatite (apatite beforsite I and II), Niocorp logged this rock as dolomite carbonatite with locally abundant apatite mineralization. The photomicrograph in Fig. 3 is of dolomite carbonatite, representing of the volumetrically abundant rock unit.

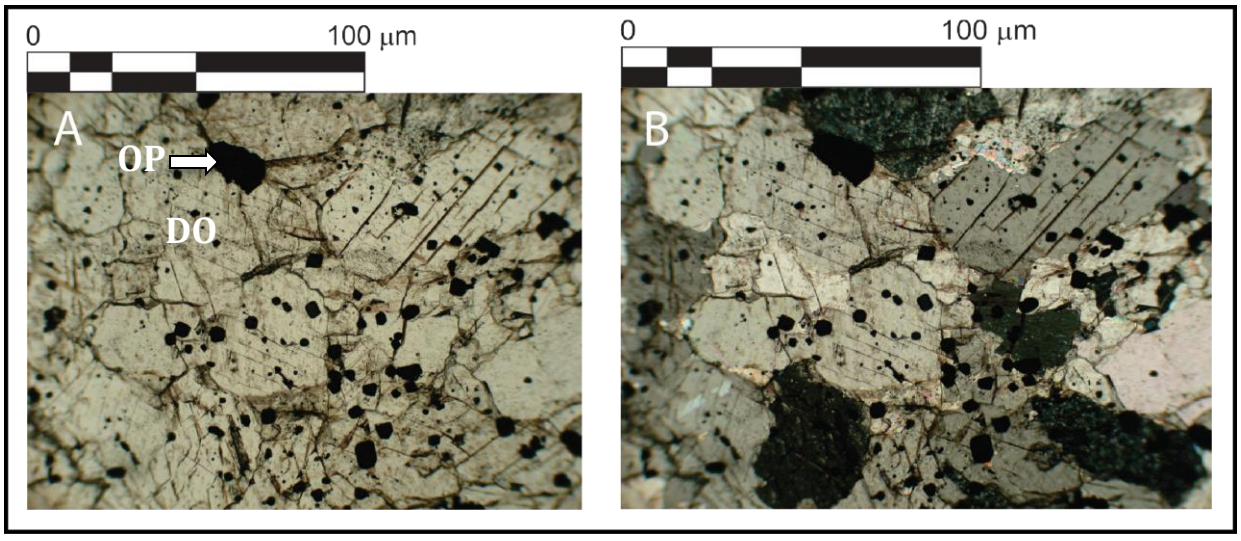

Fig. 3. Photomicrograph of dolomite carbonatite, light colored dolomite (**DO**) grains and opaque (**OP**) minerals, in (A) plane polarized light and (B) crossed polars, void of apatite. Unpublished images are courtesy of Dr. Richard Kettler.

Fig. 4 is an interpretation of the paragenetic sequence of the ECCC by Blessington (2014). He based this sequence on unit contacts and crosscutting relationships observed in core and historic drill logs. The unit names and unit descriptions (Blessington, 2014) in Fig. 4 are equivalent to the present day names in Table 1, and rock descriptions used in this research.

Fig. 4. Proposed paragenetic sequence by Blessington (2014) of the ECCC. The thickness of the lines represents the volumetric abundance of each unit.

4.1 Dolomite Carbonatite

The dolomite carbonatite is the most abundant rock type in the system (Fig. 5). Dolomite is the primary rock-forming mineral and barite, hematite, fluorite, magnetite, ilmenite, pyrochlore, pyrite, and chalcopyrite are accessory minerals. Three textures can be found in the ECCC. (1) *Massive* texture which is typically holocrystalline with equant dolomite grains in thin section (Blessington, 2014; Xu, 1996). (2) *Fine-grained flow banded* texture where the flow banding interchanges between a cream (2.5YR 8.5/2) dolomite carbonatite and a cream dolomite carbonatite with elongated red hematite grains. (3) *Coarse-grained breccia* contains

clasts of magnetite-dolomite carbonatite and mafic dike. In unaltered intervals the color can range from cream to light and dark shades of grey (N7/+0.75 to N4/+0.5, respectively). Samples were collected from the massive dolomite carbonatite and the dolomite carbonatite breccia.

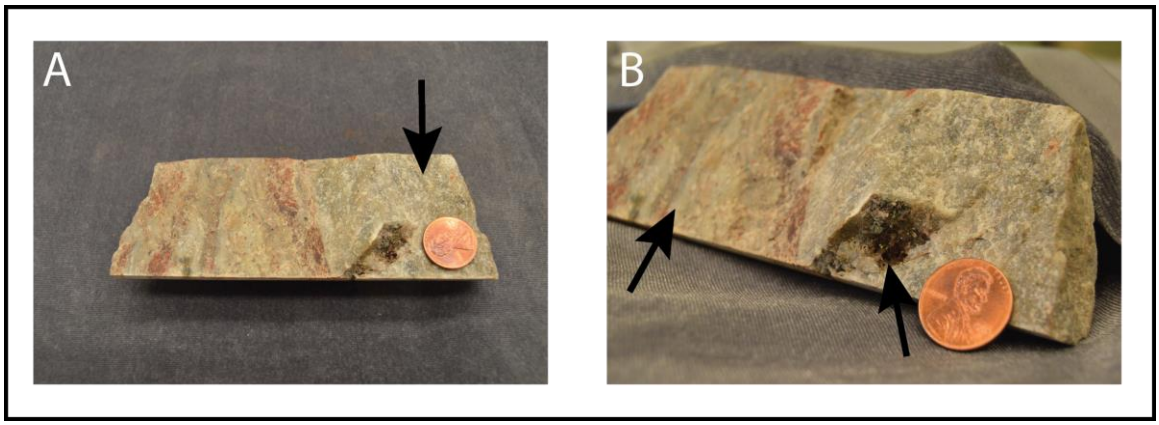

Fig. 5. Massive dolomite carbonatite core with a barite-dolomite carbonatite vein. (A) Arrow points to dolomite carbonatite (B) Arrow on the left pointing to barite-dolomite carbonatite, and the arrow on the right points to a small vug filled with barite and chalcopyrite.

4.1.2 Magnetite-Dolomite Carbonatite

The magnetite-dolomite carbonatite is the primary host for niobium-bearing pyrochlore mineralization. Blessington (2014) was able to identify the major rock forming minerals as magnetite, dolomite, ilmenite, and barite with minor apatite, rutile, biotite, quartz, and pyrochlore using backscattered electron imaging and energy dispersive spectrometry. Barite is a widespread mineral found in the magnetite-dolomite carbonatite. It occurs in thin veins, on fracture surfaces, and disseminated within the matrix.

There are three exclusive textures of the magnetite-dolomite carbonatite. (1) The *porphyry* texture consists of elongated fine-medium grained dolomite, and is typically light grey (N7/+0.75) in color. (2) The *veinleted* texture is fine grained and can range from light grey to black (N7/+0.75 to 7.5B 2.5/4, respectively) in color. The veins typically comprise pink-red barite (2.5R 8/6 to 2.5R 5/12) or calcite, and are less than a millimeter in width. Some of the veinlets have bleached halos locally. During Niocorp's exploration project in 2014, the core was routinely scanned with a magnetic susceptibility meter. Using this tool it was determined the veinleted magnetite-dolomite carbonatite had the highest magnetic susceptibility. (3) The *brecciated* magnetite-dolomite carbonatite typically occurs locally where a mafic or lamprophyre dike has intruded into the unit. The breccia matrix can range from light grey to black (N7/+0.75 to 7.5B 2.5/4, respectively) in color and is coarse grained with large magnetite or magnetite bearing clasts up to 5 cm (Fig. 6), and clasts of dolomite carbonatite.

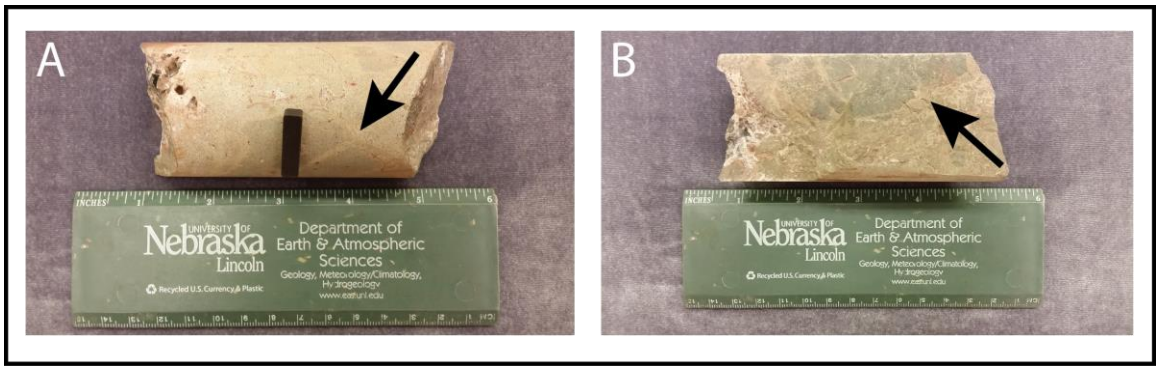

Fig. 6. Magnetite-dolomite carbonatite breccia core (A) Arrow pointing to a large magnetite grain with a magnet attached (B) Arrow pointing to the same clast as picture (A), however on the mechanically separated side of the core.

4.1.3 Lamprophyre and Mafic Dikes

Mafic dikes are the most abundant silicate rock type in the Elk Creek Complex. They have a porphyritic texture, and range between less than 3 cm to upwards of 100 cm thick. Carlson and Treves (2005) inferred the mafic dikes were probably tholeiitic in origin. They are very fine grained, dark olive green (7.5GY 5/2) in color, and have rounded dolomite phenocrysts. In localized areas, very thin barite veins can be observed. The mafic dikes will effervesce slightly when a 10% hydrochloric acid (HCl) solution is applied, indicating the presence of carbonate in the matrix.

Lamprophyres are intrusive silicate dikes (Fig. 7A) in the ECCC. Microscopic study of the lamprophyre shows its composition to be biotite, orthoclase, dolomite, apatite, and opaque minerals, with trace amounts of chlorite, barite, and quartz (Xu, 1996). The biotite is readily seen in hand specimen and can be as large as 3 cm (Fig. 7B). The lamprophyre was inferred to be minette in origin by Carlson and Treves (2005). There are two main varieties of lamprophyre. (1) The *porphyritic* lamprophyre consists of a very fine olive green matrix (7.5GY 5/2) with phenocrysts of dolomite and biotite. The phenocrysts are usually fine to medium grained. The contact between lamprophyre and carbonatite is typically sharp.

(2) The *carbonate- bearing* lamprophyre has a very fine-to-fine grained mint green (5G 8/4) matrix, with large biotite grains. This rock unit is highly effervescent when in contact with HCl. The carbonate- bearing lamprophyre typically exists at a

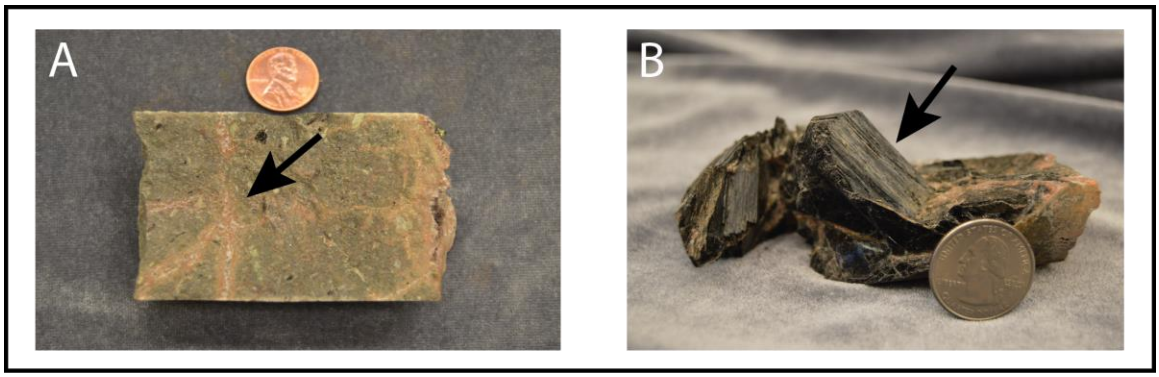

Fig. 7. (A) Lamprophyre core containing biotite (above the arrow) and the arrow is pointing at calcite veins with alteration halos (B) the arrow is pointing to what once was a large book of biotite.

gradational boundary with dolomite carbonatite; it can be as thin as 2 cm, but has also been observed in units of more than 40 m.

4.2 Mineralogy of Veins

Veining is typical in the carbonatite and mafic units, and can range in thickness from less than a millimeter to 1 m. Barite, fluorite, and minor chalcopyrite is found on fractures and vugs typically. The fluorite ranges from colorless to translucent yellow (7.5Y 6/8), and purple (2.5P 2.5m/10). Multiple carbothermal veins have been encountered in drill core. The veins comprise barite grains up to 3 cm in size, and purple (2.5P 2.5m/10) fluorite 1-2 millimeters in size, as seen in Fig. 8. The observed carbothermal veins can be up to a meter thick, with the surrounding rock being completely altered by limonite and hematite. Veins containing calcite and quartz are less common. Locally the smaller veins have

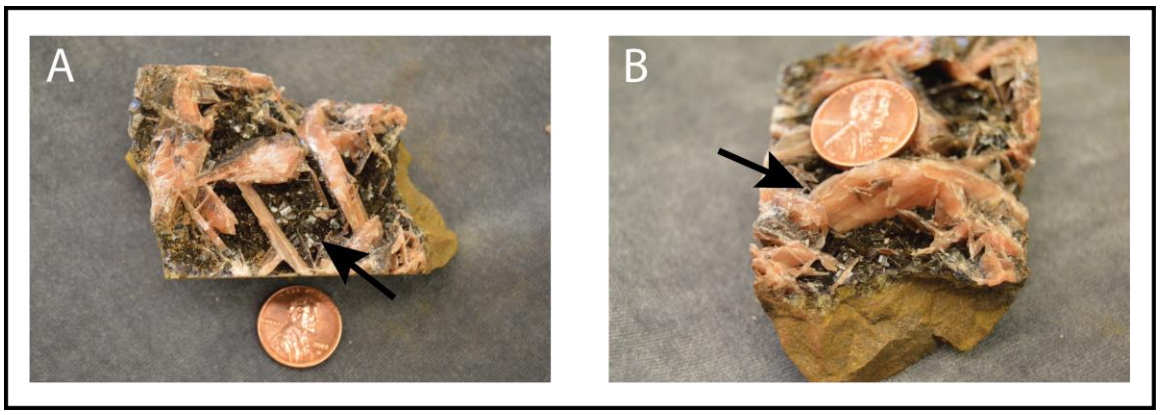

Fig. 8. Highly altered (limonite alteration) carbonatite core containing a large carbothermal vein of (A) fluorite as indicated by the arrow and (B) barite as indicated by the arrow.

bleached halos around them along with barite. In addition, thick, up to 3 meters, iron oxide veins are present, containing hematite and/or limonite.

4.3 Weathering Profile of the ECCC

While the ECCC was exposed at the surface, ~300 Ma, it was subjected to weathering processes. The weathering profile of the ECCC is as thick as 15 m. The profile consists of (1) red, pervasively slickensided illitic clays (rare) (2) red, earthy to calcite-recemented, leached saprolite, with no significant relict rock fabric (common), and (3) syenite, gneiss, or mafic rock saprock (rare) (Joeckel and Nicklen, 2007). In two of the drilled cores, a gossan-like iron cap can be observed at the upper part of the core (Nicklen and Joeckel, 2001). Illite-smectite and chlorite dominate the weathering profiles (Nicklen and Joeckel, 2001), and could be a sign of argillic alteration. The main minerals present in argillic alteration are kaolinite,

illite, and smectite (Ridley, 2013). Other minerals include biotite, chlorite, pyrophyllite, diaspore, alunite, sulfides, quartz, and andalusite (Ridley, 2013). However, Nicklen and Joeckel (2001) suggested the alteration could be a style that does not have an analogous process today.

Argillic alteration is the result of low-temperature (100-300° C) metasomatism in which clay minerals are produced through acid leaching of feldspars and mafic silicates (Ridley, 2013). The acid generated through supergene oxidation of pyrite would be sufficient to cause argillic alteration in the carbonatite complex. Nikiforov et al. (2005) describes argillization in carbonatites structurally controlled by fault zones, along with the host terrigenous rocks and gabbroids in Central Tuva.

5. Methods

5.1 Sampling

Barite and sulfide minerals were collected from each of the units described above from core available by both Molycorp and NioCorp Developments drill holes. Molycorp drill logs from the 1970's and 1980's were used to identify areas where barite and sulfides coexisted. The presence of coexisting pairs was used as necessary evidence of equilibrium between the sulfur-bearing minerals. Boxes containing the core in Mead, Nebraska were examined for barite and sulfide in contact, and those samples were extracted.

Samples from the NioCorp drill holes were collected from core obtained during the company's exploratory drill program (2014). The samples were extracted by hand, either by breaking or shaving the minerals from the rock. Each sample was given a specific ID, i.e. UNL001_barite and UNL001_pyrite for Molycorp samples, and NEC001_barite and NEC001_pyrite for NioCorp samples. No preparation was necessary for the sulfide minerals. However, the barite samples were purified to reduce the risk of contamination.

5.2 Barite Digestion

Barite was purified using the method described by Seal et al. (2000). This entailed reacting the barite with a 5 mass % solution of aqueous Na_2CO_3 at 100°C for 90 minutes to recover sulfate by ion exchange (Seal et al., 2000). Hydrochloric acid was added to reduce the pH of the solution to 4. The solution temperature was again increased to100°C and excess 10 mass % aqueous $BaCl_2$ was added and stirred continuously for 30 minutes (Seal et al., 2000). The solution was allowed to cool over night, and the barium sulfate precipitate was collected by filtration and rinsed with water the following day.

After the barium sulfate was collected, all the samples were shipped to the USGS in Reston, Virginia where Robert Seal's lab analyzed them using a continuous flow mass spectrometer. The standard used for $\delta^{34}S$ values is the Vienna Canyon Diablo troilite (VCDT) (Seal, 2006). A meteoritic value is used, because it is believed that the composition of a meteoritic sulfide mineral represents the primordial sulfur

isotopic composition of Earth (Seal, 2006). The data here are reported in the standard per mil (‰) notation defined by the following equation (Rye and Ohmoto, 1974):

$$\delta^{34}S = \left[\frac{\left({}^{34}S/_{32}S\right)_{sample} - \left({}^{34}S/_{32}S\right)_{VCDT}}{\left({}^{34}S/_{32}S\right)_{VCDT}}\right] \times 1000$$

6. Results

6.1 Sulfur Isotope Variations in the ECCC

Seventy-four samples of sulfide and barite were collected from the Elk Creek Carbonatite Complex. Sulfur isotope analysis was conducted on 64 samples; 1 sample was lost during barite digestion and the other 9 were unable to be processed at the USGS due to size limitations. Of the 64 samples, there are 24 pairs of coexisting barite and sulfide. This is the largest sulfur isotope dataset for any carbonatite worldwide. Table 2 shows the values of all sulfide and barite sampled within the system, along with lithology. The overall range for $\delta^{34}S$ values in the ECCC is -11.89‰ to +16.67‰ for sulfates and sulfides measured.

Table 2 $\delta^{34}S$ values of sulfate and sulfide minerals, and rock type the sample was retrieved.

Sample	$\delta^{34}S_{ba}$	$\delta^{34}S_{py}$	$\delta^{34}S_{cpy}$	Rock Type
MOLYCORP SAMPLES:				
UNL001	-5.76	-5.81		dolomite carbonatite
UNL002		-7.58		dolomite carbonatite
UNL003	10.97			lamprophyre breccia
UNL004	-6.75		-3.44	dolomite carbonatite
UNL005	3.75		0.05	mafic
UNL006	-6.74		-5.32	lamprophyre breccia
UNL007			-5.86	lamprophyre breccia
UNL008			-5.58	lamprophyre breccia
UNL009	-6.91		0.00	magnetite-dolomite carbonatite
UNL010	-5.57		-0.23	magnetite-dolomite carbonatite
UNL011	-6.38		-10.85	dolomite carbonatite
UNL012	-5.83		-7.04	magnetite-dolomite carbonatite
UNL013	-6.11		-4.66	magnetite-dolomite carbonatite breccia
UNL014	-6.98		-5.03	magnetite-dolomite carbonatite breccia
UNL015	-5.31		-4.93	magnetite-dolomite carbonatite breccia
UNL016	-5.41		-7.10	lamprophyre
UNL017	-6.23		-10.29	lamprophyre breccia
UNL018	-6.02		-7.94	dolomite carbonatite
UNL019	-6.68		-7.92	dolomite carbonatite
UNL020	-5.68		-4.73	magnetite-dolomite carbonatite breccia
UNL021	-4.60		-0.13	magnetite-dolomite carbonatite breccia
UNL022	-6.93		0.06	magnetite-dolomite carbonatite breccia
EC27_001	-6.71		-6.56	dolomite carbonatite breccia
EC27_001_2	-5.66			dolomite carbonatite breccia
EC27_001_3				dolomite carbonatite breccia
EC27_002	12.58			lamprophyre breccia
EC27_003	-5.3			lamprophyre breccia
EC27_003_2	1.02			lamprophyre breccia
EC27_004	-4.31			lamprophyre breccia
EC27_005	16.67			lamprophyre breccia
EC27_006				dolomite carbonatite breccia
EC28_001_2	-11.55			magnetite-dolomite carbonatite breccia
EC28_002				magnetite-dolomite carbonatite breccia
EC28_003	-8.07		-3.93	magnetite-dolomite carbonatite breccia
EC28_003_2				magnetite-dolomite carbonatite breccia
EC28_003_3	-11.89			magnetite-dolomite carbonatite brecci
NIOCORP SAMPLES:				
NEC001	10.99	-5.06		magnetite-dolomite carbonatite breccia
NEC002	1.77	-2.77		magnetite-dolomite carbonatite breccia
NEC003	9.47	-4.14		magnetite-dolomite carbonatite breccia
NEC004	11.06	-5.83		magnetite-dolomite carbonatite breccia
NEC005		2.26		magnetite-dolomite carbonatite
NEC006		0.6		magnetite-dolomite carbonatite
NEC007		2.31		magnetite-dolomite carbonatite
NEC008	0.99			magnetite-dolomite carbonatite

ba- barite, **py**- pyrite, and **cpy**- chalcopyrite

6.1.2 Sulfur Isotope Variations by rock type

The $\delta^{34}S$ values vary greatly in each rock unit, except for the dolomite

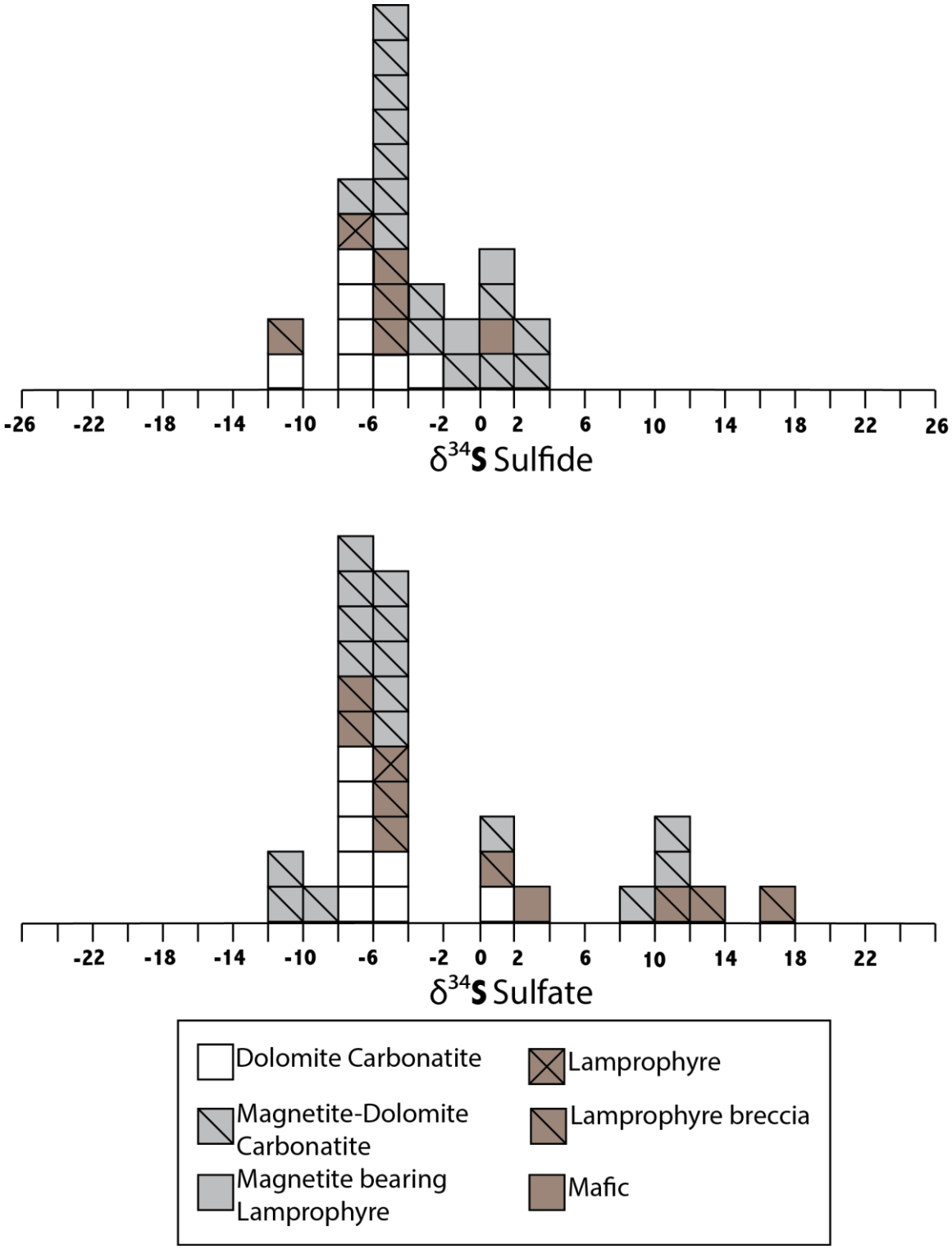

Fig. 9. Distribution of $\delta^{34}S$ values by rock type and mineralization. Each box represents one sample.

carbonatite. Fig. 9 contains two histograms, one for sulfide and the other sulfate, illustrating the distribution of $\delta^{34}S$ values by rock type. $\delta^{34}S$ values for sulfides range from -10.85‰ to +2.31‰, and $\delta^{34}S$ values for sulfates range from -11.55‰ to +16.67‰. The sulfates also form two distinctive groups, ^{34}S enriched and ^{34}S depleted where 0‰ is the dividing boundary between them (Fig. 9).

6.2 Iron Oxide Alteration Profiles

Two profiles were created to map alteration in the ECCC (Fig. 10). Note that the profiles only represent the presence of iron oxide alteration and do not indicate its pervasiveness in the core. The locations of A-A` and B-B` can be seen in the map below (Fig. 11). Profile A-A` is an east (E) to west (W) trending intersection that cuts through the diameter of the carbonatite including the zone of mineralization; the drill holes are rather spread out, the largest distance between two holes being 2110.52 meters. Profile B-B` is a northwest (NW) to southeast (SE) trending intersection that is predominantly in the zone of mineralization. The largest distance between drill holes in profile B-B` is 310.16 m. Table 3 indicates the inclination and trend of the drill holes. Molycorp's drilling was oriented to intersect the complex from the northwest and southeast, with a couple exceptions. All of NioCorp's drilling was oriented to intersect the complex southwest to northeast, with the exception of two holes, including NEC-011.

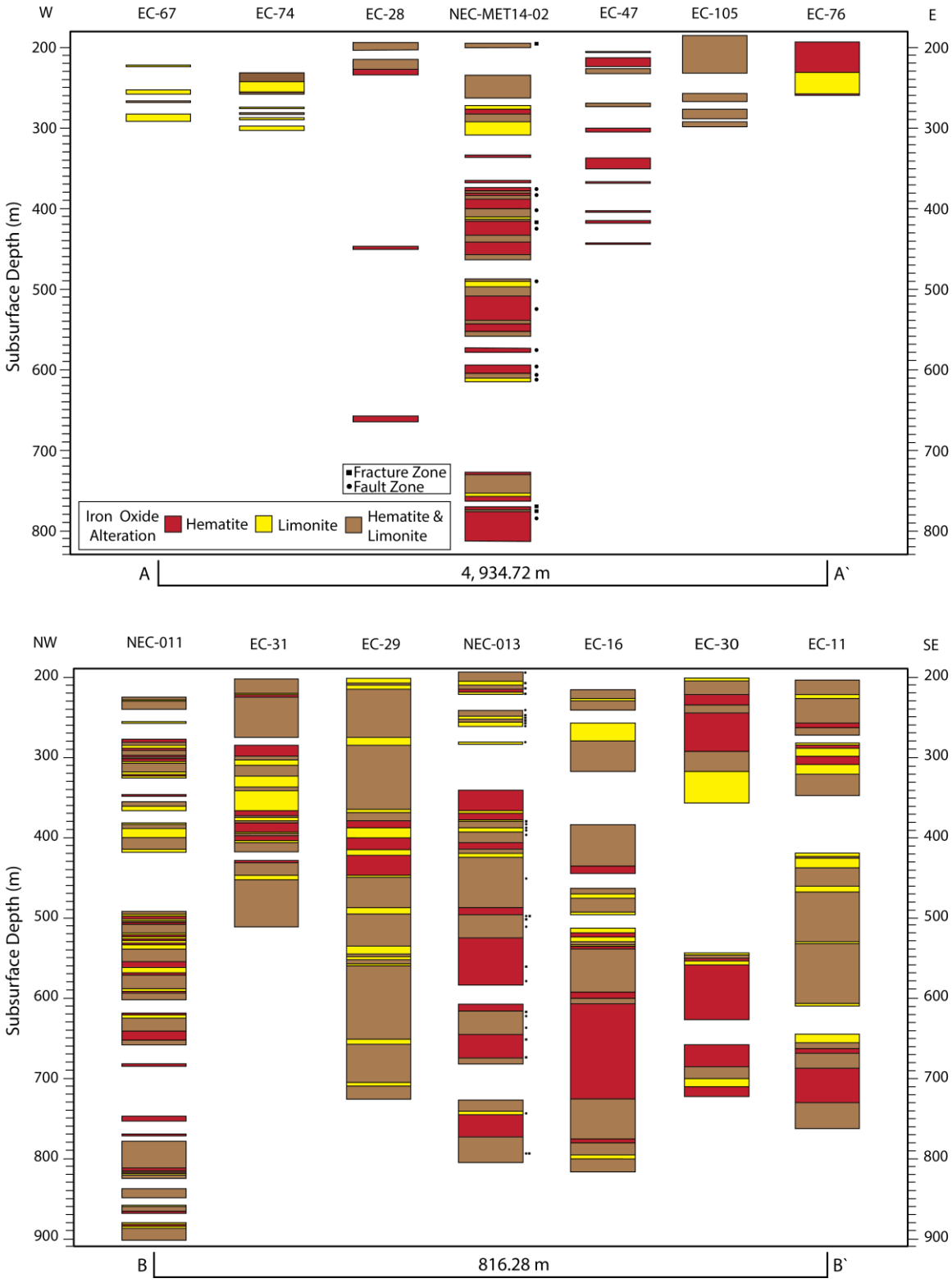

Fig. 10. A-A` and B-B` profiles intersect the Elk Creek Carbonatite Complex showing iron oxide alteration and fault/fracture zones down hole. Fault/fracture zones retrieved from unpublished Niocorp drill logs. The horizontal scale is the length of each transect.

Using iron oxide profiles A-A` and B-B` (Fig. 10), a general trend can be seen within the alteration. In profile A-A` it appears the amount of hematite alteration increases toward the east; it appears there is a slight increase at depth too, but since there are only two holes that go beyond 450 m that can not be said with certainty. However, in profile B-B` it does appear as though hematite alteration does increase at depth. B-B` also displays a NW-SE trend where hematite alteration increases to the SE. These trends prelude to alteration being structurally controlled.

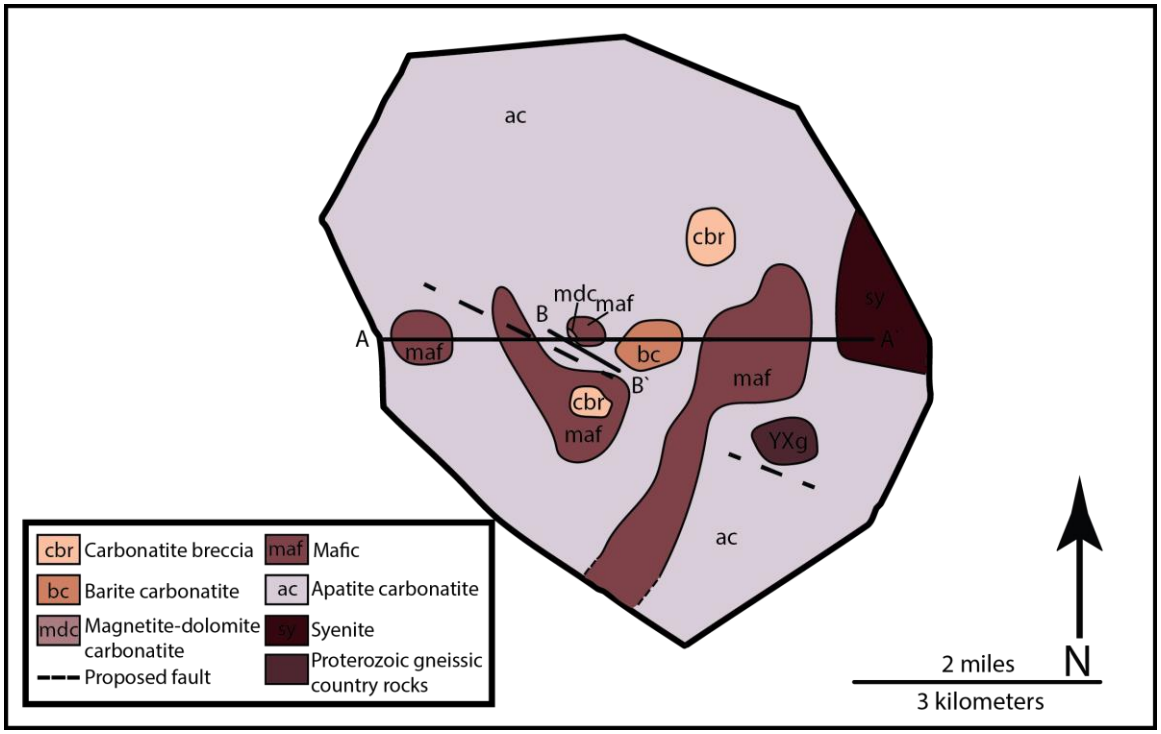

Fig. 11. Location of profile intercepts (A-A` and B-B`) and rock units that make up the carbonatite complex. The outer boundary is based on Molycorp drill logs, and rock unit boundaries are adapted from Drenth (2014). For nomenclature purposes in this research **apatite carbonatite** (not sampled for this research)= dolomite carbonatite, **carbonatite breccia**= dolomite carbonatite breccia, and **barite carbonatite** (not sampled for this research)= altered dolomite carbonatite; **magnetite dolomite carbonatite** and **mafic** rocks match the rock units in this research.

Table 3 Inclination and trend of the core used for the iron oxide alteration cross sections.

Location	Hole ID	Inclination	Trend
A-A`			
	EC-28	-90	NW-SE
	EC-47	-60	—
	EC-67	-90	—
	EC-74	-90	—
	EC-76	-90	—
	EC-105	-90	—
	NEC-MET14-02	-90	SW-NE
B-B`			
	EC-11	-62	NW-SE
	EC-16	-60	NW-SE
	EC-29	-90	NW-SE
	EC-30	-90	N
	EC-31	—	S
	NEC-011	-65	NW-SE
	NEC-013	-90	SW-NE

7. Discussion

$\delta^{34}S$ variations in the ECCC are a result of several factors, including (1) origin of magma from the mantle (2) sulfur degassing, and (3) post-magmatic supergene alteration. Supergene also explains anomalously high strontium ratios. In addition, the groundwork has been laid for mapping and interpretation of iron oxide alteration. It is important to identify hematite alteration because it weakens the rock, which could compromise the stability of a mine, and the alteration also affects rare earth elements (REEs) mobilization.

7.1 Hypogene Sulfur Isotopes and Applications

Hypogene $\delta^{34}S$ values for sulfides in the ECCC (-10.85‰ to +2.31‰) are consistent with sulfur isotope values for sulfides in carbonatites worldwide. Gomide et al. (2013) reported $\delta^{34}S$ values for sulfides for the Jacupiranga complex carbonatites ranging from -6.1‰ to -3.2‰, and from -24.6‰ to -2.2‰ for the Alto Paranaiba Igneous Province (APIP) in Brazil, which contains six carbonatites including: Catalão I and II, Serra Negra, Salitre, Araxá, and Tapira. Mitchell and Krouse (1975) complied $\delta^{34}S$ values for sulfides in the Mountain Pass, Bearpaw Mountains, Magnet Cove, Oka, and Phalaborwa carbonatites, and found $\delta^{34}S$=-11‰ to +5‰. Drüppel et al. (2006) measured $\delta^{34}S$ values for sulfides for the Swartbooisdrif ferrocarbonatite in Namibia that range from -3.3‰ to +5.1‰.

Positive $\delta^{34}S$ values of sulfate, +1.77‰ to +11.06‰, are also similar to values of hypogene minerals found in carbonatites worldwide. Therefore, the positive $\delta^{34}S$ values for sulfates are considered to be hypogene in origin in the ECCC. Mitchell and Krouse (1971) found $\delta^{34}S$ values for barite to range from +1.3‰ to +7.2‰ from Mountain Pass. Gomide et al. (2013) presented $\delta^{34}S$ values for sulfates that range from -3.9‰ to +12.9‰ from several carbonatites in the APIP and Jacupiranga carbonatite complexes; one sample from Tapira reaching 16.8‰, however, it was considered to be of secondary origin.

The Phalaborwa (or Palabora) Complex, located in South Africa, has become somewhat of an unofficial standard for carbonatites. It is considered to be of mantle origin with little variation in $\delta^{34}S$ sulfide values, the range being 2.1‰ ± .8 (von

Gehlen, 1967). The sulfur isotope composition for bulk earth is generally considered 0 ± 2‰ (Chaussidon et al., 1987; Seal, 2006). Phalaborwa is also void of barite and other sulfates, indicating little variation in redox environments. When compared to Phalaborwa, Elk Creek has a highly variable sulfide-sulfur isotope composition. This does not necessarily mean sulfur in the ECCC isn't from the mantle; there are several processes during evolution that can fractionate sulfur and produce variable $\delta^{34}S$ values, such as degassing and changes in temperature. However, Deines (1989) concluded mantle heterogeneities could not be ruled out.

Likely hypogene minerals in the ECCC were identified based on physical appearance and isotopic composition. All the samples from Niocorp core (Table 2) were assumed to be in textural equilibrium with no signs of alteration (Fig. 12), and sulfates have variable but appreciable ^{34}S enrichment relative to the associated sulfide. With these samples, two applications were applied to determine temperature of formation, and the $\delta^{34}S$ value of bulk sulfur to determine its source.

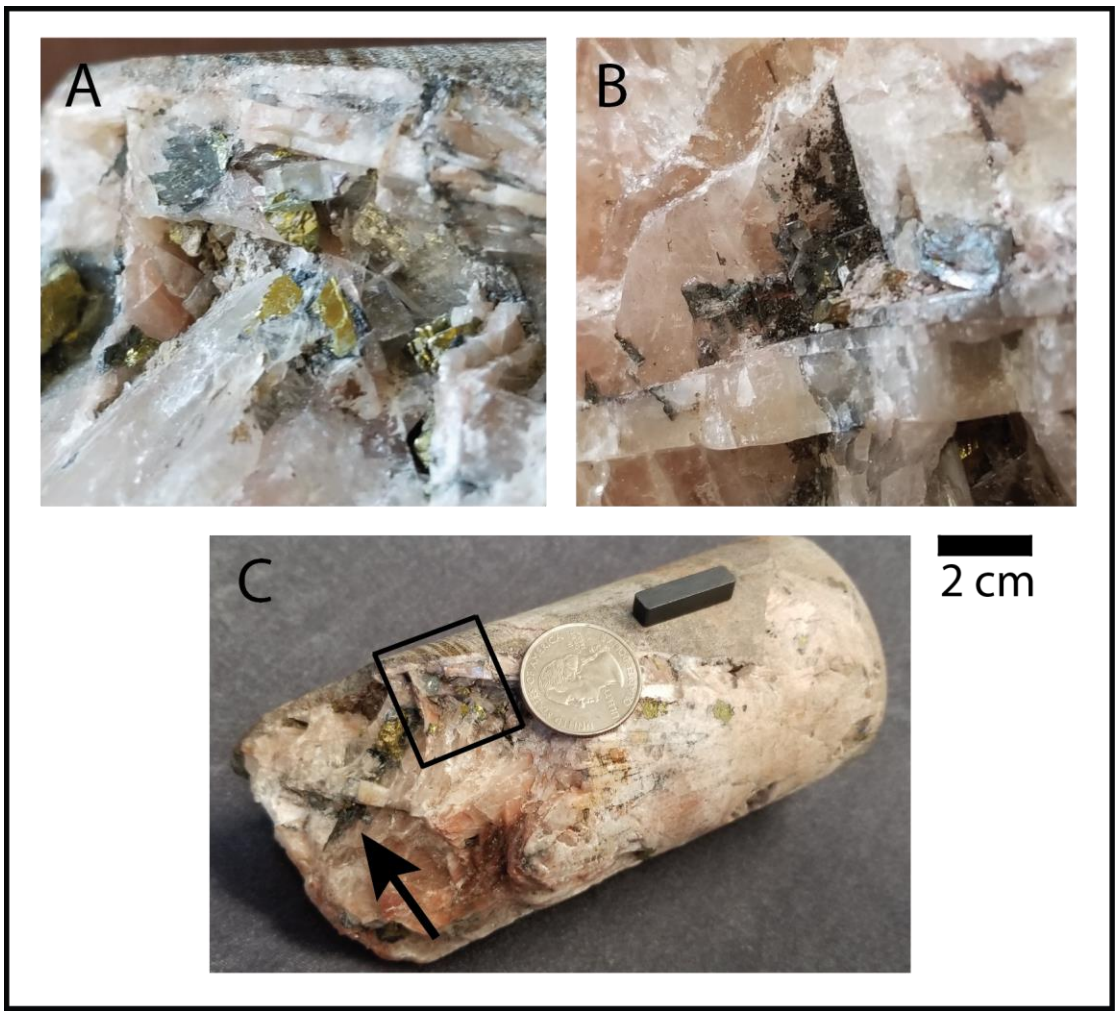

Fig. 12. Hematite mineralization in magnetite-dolomite carbonatite (A) metallic splotches of hematite in contact with barite and pyrite (B) black blebs of hematite (C) core showing the locations of A (square boundary) and B (indicated by the arrow)

Temperature was determined using the equation below from Miyoshi et al. (1984):

$$\Delta_{A-B} = 7.4\ X\ 10^6/T^2 - .19$$

where Δ_{A-B} = $\delta^{34}S_{sulfate}$ - $\delta^{34}S_{sulfide}$ and T= temperature in °C. Miyoshi et al. (1984) experimentally showed that sulfide and sulfate fractionation factors obey the above equation in the temperature range of 600°C -1000°C. The temperatures obtained are 675°C, 730°C, 660 °C, and 1250°C; Table 4 displays the sulfur pairs with their respective temperature. Aside from 1250°C, these formation temperatures are similar to ones obtained from other carbonatites worldwide (Gomide et al., 2013), and experimentally (Wyllie, 1966). It has been previously observed that as temperatures cool, sulfur fractionation between sulfate-sulfide sulfur pairs increases (Seal, 2000; Gomide at al., 2013). Gomide et al. (2013) were able to track

Table 4 $\delta^{34}S$ values and temperatures for primary sulfate and sulfide.

Sample	$\delta^{34}S$ (‰)	Temperature (°C)
NEC001_barite	10.99	675
NEC001_pyrite	-5.06	
NEC002_barite	1.77	1250
NEC002_pyrite	-2.77	
NEC003_barite	9.47	730
NEC003_pyrite	-4.14	
NEC004_barite	11.06	660
NEC004_pyrite	-5.83	

early to late stage magma evolution using barite and sulfide pairs from carbonatites in Brazil. Gomide et al. (2013) traced evolution starting at an early stage crystallization temperature of ~675 °C using pairs from Catalão I, and ending with late stage pairs from Catalão I yielding a temperature of ~459 °C. After Gomide et al. (2013), samples taken from the ECCC appear to resemble early stage crystallization/formation, as seen in Fig. 13. Blessington's (2014) places magnetite-dolomite carbonatite emplacement relatively early in the sequence (Fig. 4), which is now confirmed by the formation temperatures presented here.

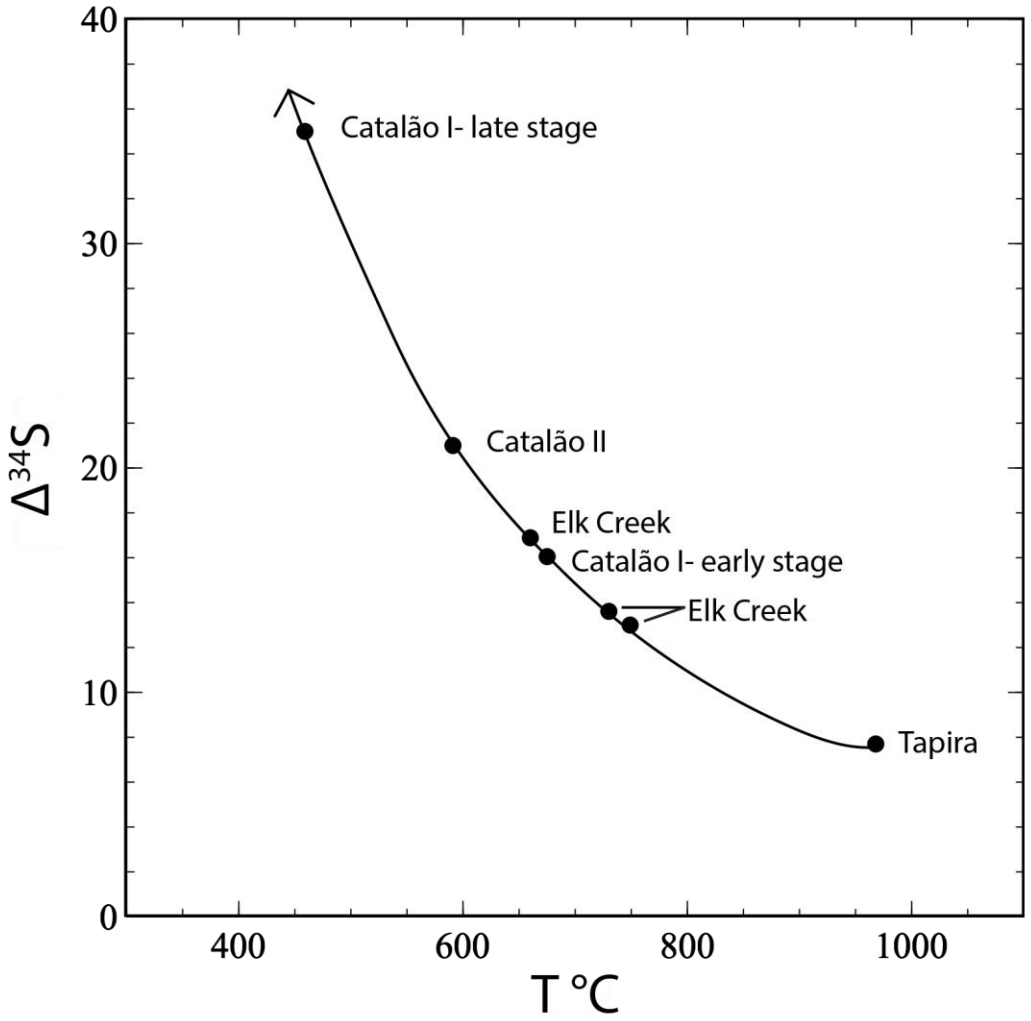

Fig. 13. $\Delta^{34}S$ vs. temperature data are from Gomide et al. (2013) for all carbonatites except Elk Creek. All temperatures were determined by the equation listed above from Miyoshi et al. (1984). The arrow is indicating the evolution path.

Since hematite, barite, and pyrite occur in the same vein, we were able to determine log fO_2 and log fS_2. Using the equations from Table 5, log K was determined at a pressure of 1 kilobar and temperature at 730 °C. Wyllie and Tuttle (1958) showed that calcite begins to melt in the ternary system CaO-CO_2-H_2O at a temperature of 740°C and 1000 bar pressure. Temperature was determined from sample NEC_003. One kilobar pressure is commonly used in experimental studies of carbonatites. Also, isotopic evidence has been provided showing S is mainly present as sulphide in carbonatite magmas with temperatures of 700 °C or higher (Wyllie, 1989).

After log K was calculated for each equation, log fO_2 and log fS_2 for the hematite-magnetite (HM) boundary were determined to be -11.36 and 0.975, respectively. Using mole fractions determined by $\delta^{34}S$ values from sample NEC003, assuming Raoult's law applies, log fO_2 of -15.26 was determined for the SO_2-H_2S boundary listed in Table 4.

Table 5 Equations for stability field boundaries for the Fe-O-S system.

Boundary	Reaction	log K Temp. 730 °C	Equation of log fO_2 or log fS_2
$Fe \rightarrow FeS$	$Fe + .5\ S_2 \rightarrow FeS$	4.94	$\log fS_2 = -9.88$
$FeS \rightarrow FeS_2$	$FeS + .5\ S_2 \rightarrow FeS_2$	0.17	$\log fS_2 = -0.346$
$Fe \rightarrow Fe_3O_4$	$3\ Fe + 2\ O_2 \rightarrow Fe_3O_4$	41.02	$\log fO_2 = -20.51$
$Fe_3O_4 \rightarrow Fe_2O_3$	$2\ Fe_3O_4 + 0.5\ O_2 \rightarrow 3\ Fe_2O_3$	5.68	$\log fO_2 = -11.36$
$FeS \rightarrow Fe_3O_4$	$3\ FeS + 2\ O_2 \rightarrow Fe_3O_4$	26.19	$\log fO_2 = .75 \log fS_2 - 13.10$
$Fe_3O_4 \rightarrow FeS_2$	$Fe_3O_4 + 3\ S2 \rightarrow 3\ FeS2 + 2\ O_2$	-25.67	$\log fO_2 = 1.5 \log fS_2 - 12.84$
$Fe_2O_3 \rightarrow FeS_2$	$Fe_2O_3 + 2\ S_2 \rightarrow 2\ FeS_2 + 1.5\ O_2$	-19.01	$\log fO_2 = 1.3 \log fS_2 - 12.67$
$SO_2 \rightarrow H_2S$	$SO_2 + H_2O \rightarrow H_2S + 1.5\ O_2$	-22.90	$\log fO_2 = -15.26$

Log K data calculated at 730°C and 1 kbar using SUPCRT92 (Johnson et al. 1992) with slop16.dat thermodynamic database (http://geopig.asu.edu/sites/default/files/slop16.dat).

Using Table 5, a phase diagram for the Fe-O-S system was created (Fig. 14). The value of a_{SO2}/a_{H2S} increases from the SO_2-H_2S boundary with increasing fO_2. This indicates the barite, pyrite, and hematite precipitated from a sulfate-dominated fluid. If the system was not in equilibrium, the $\delta^{34}S_{\Sigma S}$ value could be interpreted to be that of the sulfate. However, the pyrite and barite in this system are expected to be in equilibrium. Ohmoto and Goldhaber (1997) determined that at temperatures

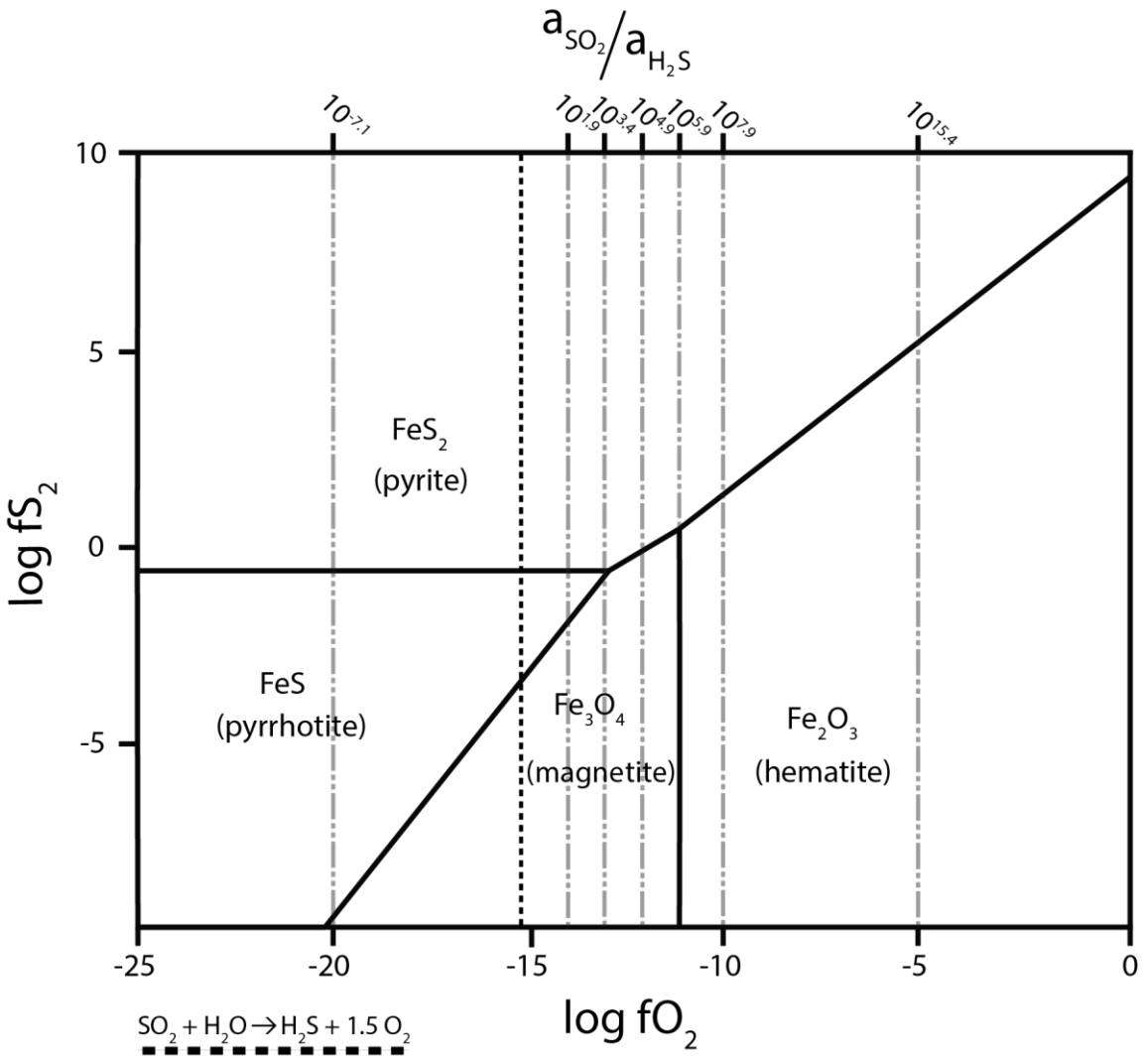

Fig. 14. Fe-O-S phase diagram constructed from the equations in Table 4.

greater than 200°C, where all sulfur species are assumed to be in equilibrium prior to deposition, the $\delta^{34}S$ value of H_2S and ΣSO_4 do not always indicate the origin of the sulfur in the fluid. The proportion of oxidized and reduced aqueous sulfur species, the equilibrium fractionation factors between them, and the $\delta^{34}S_{\Sigma S}$ value must be evaluated using the equation (Ohmoto and Goldhaber, 1997):

$$\delta^{34}S_{\Sigma S} = \delta^{34}S_{H_2S} + \Delta_{SO_4-H_2S}\left(\frac{R}{1+R}\right)$$

where R is the mole ratio of the oxidized and reduced sulfur in solution. Since the samples had temperatures above 350°C, calculations were made using SO_2 instead of SO_4, because at those temperatures it would be the dominant oxidized species (Ohmoto and Goldhaber, 1997). Using the same sample to illustrate Fig. 14 (NEC003 from Table 3) and samples NEC001 and NEC004 (Table 6), the range for $\delta^{34}S_{\Sigma S}$ values is -2.23‰ to -1.64‰, which is within the ±2‰ range for typical mantle sulfur (Chaussidon et al., 1987; Seal, 2006). This range is slightly deviated from 0‰, which could indicate local heterogeneities in the mantle (Deines, 1989; Chaussidon et al., 1987).

Table 6 $\delta^{34}S_{\Sigma S}$ determined using the SO_2-H_2S equilibrium fractionation isotopic factor from Ohmoto and Rye (1979).

Sample	$\delta^{34}S$ (‰)	$\delta^{34}S_{\Sigma S}$ (‰)
NEC001_barite	10.99	-1.92
NEC001_pyrite	-5.06	
NEC002_barite	1.77	———
NEC002_pyrite	-2.77	
NEC003_barite	9.47	-1.64
NEC003_pyrite	-4.14	
NEC004_barite	11.06	-2.23
NEC004_pyrite	-5.83	

7.2 Degassing Effects on Sulfur Isotope Fractionation

The main two sulfur species in a melt are SO_2 and H_2S (Ohmoto and Goldhaber, 1997). The outgassing of these species can cause the abundance of ^{34}S in the melt to change, shifting the $\delta^{34}S$ values to more positive or negative values (Yongfei, 1990). Outgassing of SO_2 and/or H_2S is dependent on several variables: temperature, fO_2, the sulfate/sulfide ratio and mole fraction of sulfide in the melt, and the fraction of sulfur remaining in the melt (Yongfei, 1990; Marini et al., 2011). The following two sections (7.2.2 and 7.2.3) are a summary of Marini et al's. (2011) experiments illustrating the effects of outgassing on $\delta^{34}S$ values of the residual melt. Marini et al. (2011) conducted the experiments at temperatures of 1200°C and 900°C. The following results characterize effects at 900°C (Fig. 15); this temperature was chosen because it is closer to carbonatite formation temperatures than 1200°C.

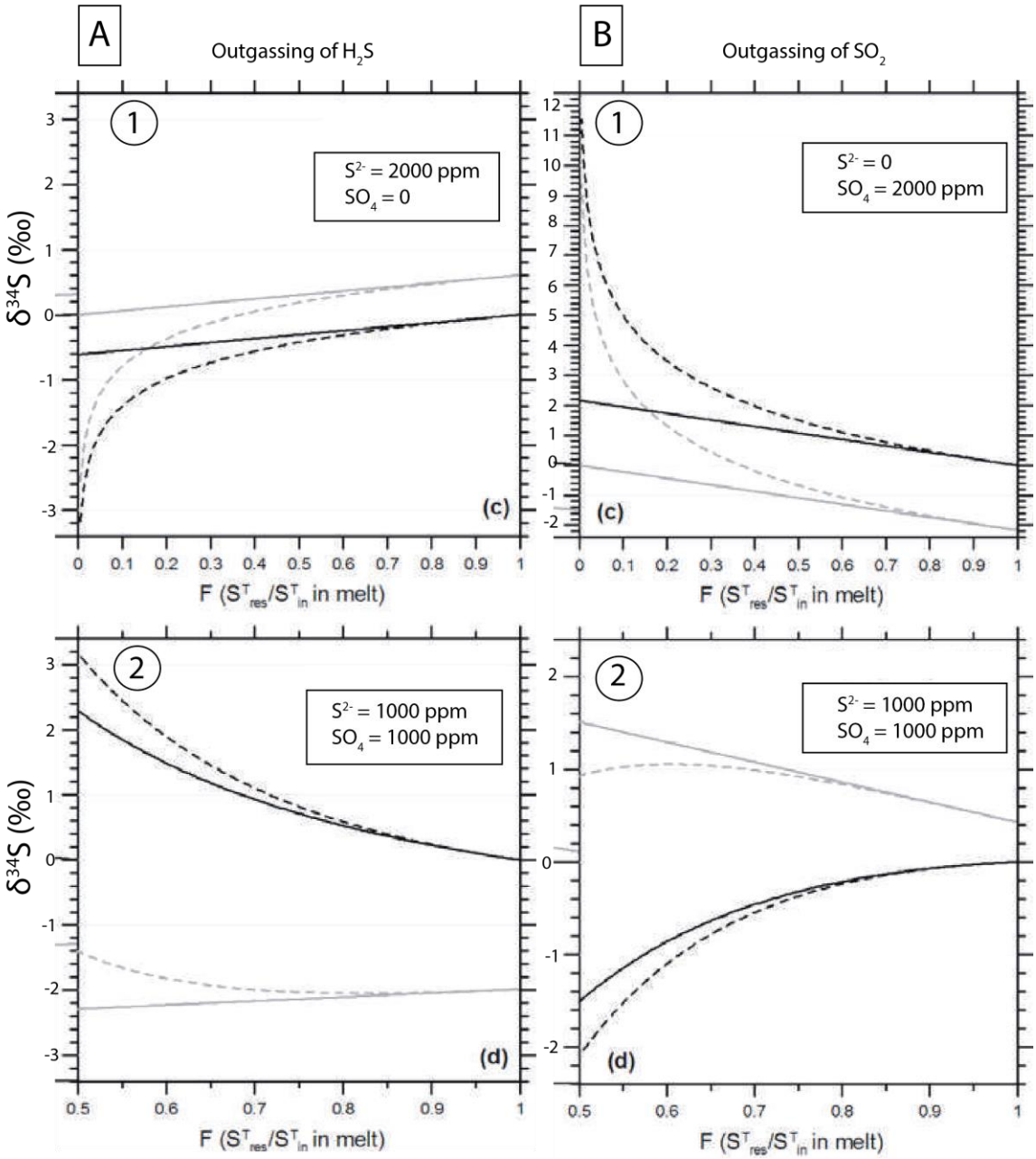

Fig. 15. Adapted from Marini et al. (2011). The black lines indicate the melt phase, and the grey lines represent the gas phase. The dashed and solid lines represent an open- and closed-system, respectively. F = the fraction of sulfur remaining in the melt.

7.2.2 Outgassing of SO_2

Marini et al. (2011) concluded that the fractionation of sulfur isotopes during outgassing (in an open or closed system) is controlled by the values of $Y_{SO_4^{2-}}$ and Y_{SO_2}, where $Y_{SO_4^{2-}} = X_{SO_4^{2-}}/(X_{SO_4^{2-}} + X_{S^{2-}})$ and $Y_{SO_2} = X_{SO_2}/(X_{SO_2} + X_{H_2S})$. In the first experiment, $Y_{SO_4^{2-}} = 1$ and no sulfide is present. The outgassing of SO_2 produced an increase in $\delta^{34}S$ values for both the gas and silicate melt as the fraction of sulfur remaining in the melt decreased (Fig. 15B-1) (Marini at al., 2011).

Scenario two from Marini et al. (2011) describes a system where sulfate and sulfide exist in equal proportions ($Y_{SO_4^{2-}} = 0.5$). In this system, the $\delta^{34}S$ value of the melt decreases when SO_2 is outgassed, and the fraction of sulfur remaining in the melt decreases (Fig. 15B-2).

7.2.3 Outgassing of H_2S

Outgassing of H_2S can also affect the $\delta^{34}S$ values of sulfur remaining in a melt. Marini et al. (2011) showed the effects of H_2S outgassing using two different scenarios where oxidation state is not fixed. In the first experiment, all the dissolved sulfur was present as the sulfide ion (S^{2-}), so $Y_{SO_4^{2-}} = 0$. In this case, as the fraction of sulfur remaining in the melt decreases, the $\delta^{34}S$ value of the residual melt also decreases (Fig. 15A-1).

In the second scenario from Marini et al. (2011), the sulfur is partitioned in equal proportions between S^{2-} and SO_4^{2-} ($Y_{SO_4^{2-}}$ = 0.5). The results show the opposite of the first scenario where the melt, in this case, is enriched in ^{34}S, and as the fraction of sulfur remaining in the melt decreases the $\delta^{34}S$ value of the melt increases (Fig. 15A-2).

7.2.4 Effects of Degassing in the Elk Creek Carbonatite Complex

The $\delta^{34}S$ values for the samples NEC005, NEC006, and NEC007 are +2.26‰, +0.6‰, and +2.31‰, respectively. These values are significantly more enriched in ^{34}S than the remainder of the hypogene sulfide samples and are used as evidence for degassing in the ECCC. Textural evidence suggests that the samples were retrieved from core that underwent degassing. The three samples were collected from a vug that was located in an altered, brecciated magnetite-dolomite carbonatite. The minerals present in the vug were barite, pyrite, and trace hematite and fluorite.

The presence of both sulfate and sulfide minerals immediately eliminates the two scenarios from Marini et al (2011) where only sulfate or sulfide were present during outgassing (Fig. 15 A-1 and B-1). The second scenario during the outgassing of SO_2, where sulfate and sulfide are both present, can also be eliminated because the residual melt is depleted in ^{34}S (Fig. 15B-2). It is likely the pyrite samples with appreciable ^{34}S precipitated in an environment similar to the second scenario during the outgassing of H_2S (Fig. 15A-2). As S^{2-} is lost as gaseous H_2S, the residual fluid is enriched in ^{34}S, precipitating sulfur-bearing minerals with higher $\delta^{34}S$ values.

7.3 Supergene Alteration: Background

Supergene alteration typically occurs at or near the Earth's surface. However, supergene alteration can range to great depths, up to kilometers (Morris, 1983; Wiliams, 1990); Nikiforov et al. (2006) reported an oxidation zone that reaching depths of 300m in Karasug field carbonatites. Metals leached by meteoritic waters are carried downward by percolating groundwater and deposited in a zone of enrichment at the hypogene/supergene boundary. Supergene enrichment is thus a very important process in creating economically viable ore deposits that otherwise would not have been. In the use of research, supergene alteration is an important tool in identifying geologic processes that alter mineral deposits.

Supergene mineralization is characterized here using the findings of Field (1966). He determined that the discriminating factor between supergene and hypogene mineralization was that hypogene sulfate displays variable but appreciable ^{34}S enrichment relative to the associated sulfide, whereas supergene sulfate has a nearly identical isotopic composition to the parental sulfide.

Pyrite oxidation is a complicated process, which includes several oxidation-reduction reactions, hydrolysis and complex ion formation, and solubility controls and kinetic effects (Nordstrom, 1982). The overall process can be described by the following reaction (Rimstidt and Vaughan, 2003):

$$FeS_{2(s)} + 14\ Fe^{3+} + 8\ H_2O_{(l)} \rightarrow 15\ Fe^{2+} + 16\ H^{+} + 2\ SO_{4(aq)}$$

Breaking down the pyrite to neutral sulfur is the first step (Nordstrom, 1982). The neutral sulfur remains on the surface of the pyrite while ferrous iron leaches out. Eventually the sulfur surface becomes unstable and one of two events occurs: (1) disrupt and reorganize into elemental sulfur or (2) disrupt into solution as dimers, which would be highly unstable and form sulfate rapidly in the presence of a strong oxidizing agent (Nordstrom, 1982). Limonite is very prevalent throughout the entire ECCC, and is in close proximity to most barite samples that display supergene $\delta^{34}S$ values. Limonite is referred to as a product of pyrite oxidation for the purposes of this research. However, it typically exists as a pseudomorph from goethite.

7.3.2 Supergene Alteration: Sulfate Isotope Variation in the ECCC

A substantial number of barite samples from the Elk Creek Carbonatite Complex display $\delta^{34}S$ values that were produced by supergene alteration due to oxidation of pyrite. These samples are significantly depleted in ^{34}S compared to primary barite, and are typically nearly identical to the sulfur isotopic composition of primary sulfides.

Figure 16 illustrates the distribution of $\delta^{34}S$ values for sulfates and sulfides as a function of depth. Near the top of the intrusion from ~200 m subsurface to ~450 m, $\delta^{34}S$ values are relatively restricted. At a depth of ~500 m the $\delta^{34}S$ values for sulfates vary slightly; they vary even more at depths around 750 m. This is a good

indication of oxidizing fluids near the top of the intrusion, percolating down and depositing barite crystals with the isotopic composition of the oxidized pyrite.

Based on this interpretation, likely supergene barites have a sulfur isotopic composition ranging from -11.55‰ to -4.31‰. Compared to other carbonatites that have experienced supergene alteration, these values are significantly more

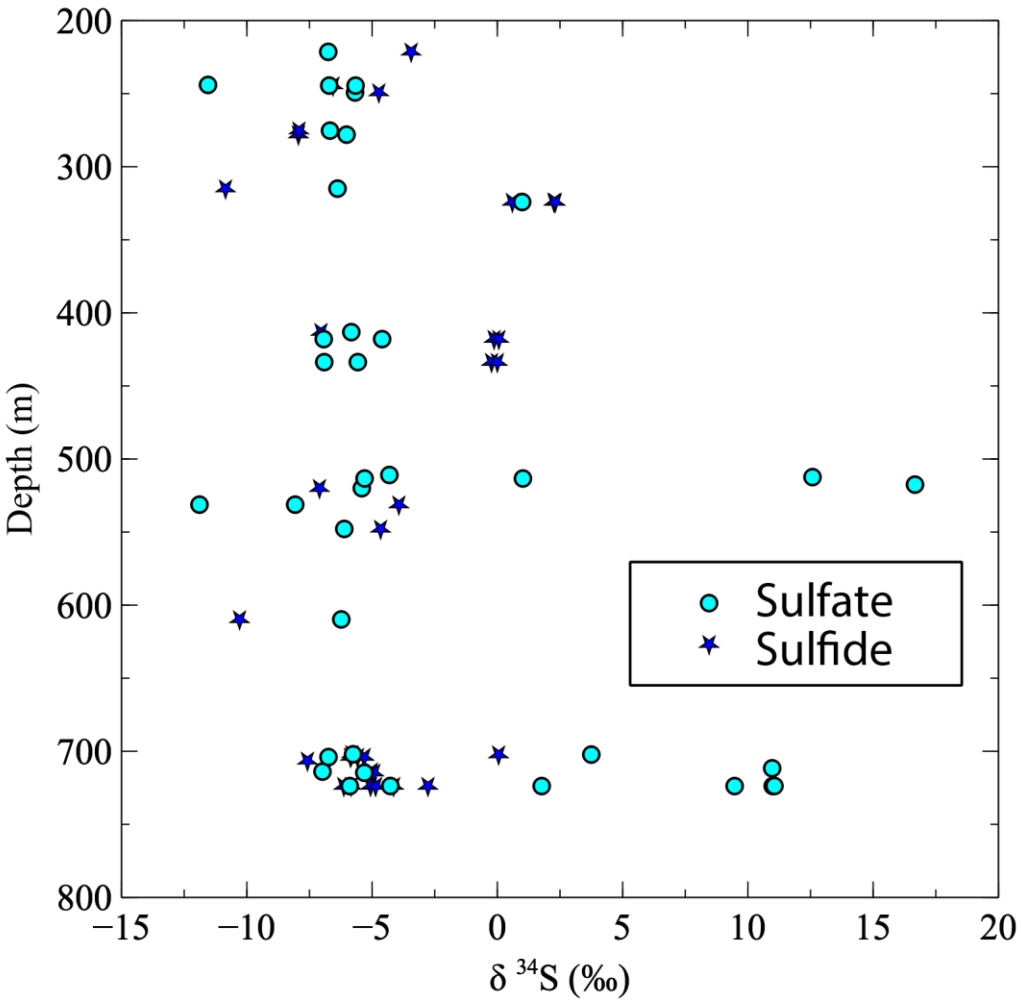

Fig. 16. $\delta^{34}S$ values for sulfur mineralization as a function of depth.

depleted in ^{34}S, such as the values reported by Nikiforov et al. (2006). The sulfides associated with the supergene sulfates are all chalcopyrite with the exception of one pyrite sample; the sulfur isotopic composition of these sulfides ranges from –10.85‰ to +0.06‰.

7.3.3 Supergene Alteration: Effects on Strontium Ratios

Brookins et al. (1975) reported strontium (Sr) ratios for 18 samples from the ECCC starting at a depth of 275.84 m through 290.17 m. All but three of the samples displayed strontium ratio values similar to carbonatites worldwide with a mean value of 0.7041, which can be explained by a mantle source (Nikiforov et al., 2006). The anomalously high $^{87}Sr/^{86}Sr$ values are 0.7085, 0.7064, and 0.7067, and cannot be explained by a mantle source. Two possible sources could be the Precambrian basement rock or Pennsylvanian sedimentary rocks.

The basement rocks surrounding the ECCC are low-to-medium-grade metamorphic gneiss and schist of island arc origin, and granitic plutons (Carlson and Treves, 2005). $^{87}Rb/^{86}Sr$ and $^{87}Sr/^{86}Sr$ values from Bickford et al. (1981b) were used to determine if the source of the radiogenic strontium was the Precambrian basement rocks. Unfortunately, no samples in that study were recovered near the carbonatite complex; the closest samples were from northern Kansas (Bickford et al. 1981a).

The Precambrian samples from Bickford et al. (1981b) had modern day $^{87}Sr/^{86}Sr$ values of 0.7474, 0.7342, and 0.7403. Using their $^{87}Rb/^{86}Sr$ and modern

day ^{87}Sr ratios, $^{87}Sr/^{86}Sr$ values were calculated for model ages of 300 Ma and 500 Ma. Figure 17 shows that the strontium evolution of the Precambrian basement rock had well exceeded even the highest anomalous $^{87}Sr/^{86}Sr$ value for the ECCC, and is unlikely the source of radiogenic Sr for these samples. However, it would only take a small amount of radiogenic Sr from the basement rocks to elevate the values in the ECCC and cannot be entirely ruled out.

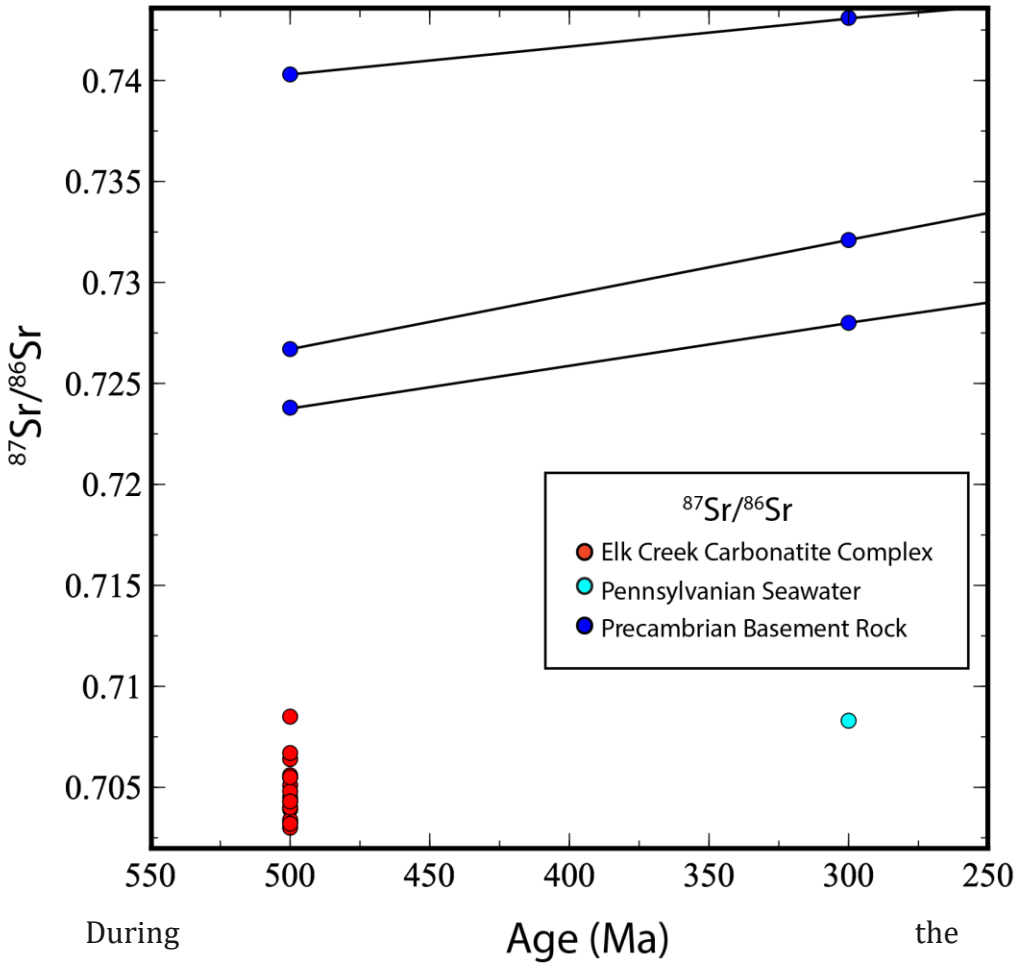

During the

Fig.17. Strontium ratios for the Elk Creek Carbonatite Complex and possible radiogenic sources Pennsylvanian Seawater (PS) and Precambrian Basement Rock (PBR). Data calculated for PBR came from Bickford et al. (1981b) and PS data is from Burke et al. (1982).

Pennsylvanian, a seaway covered Laurentia in what is the North American midcontinent. At the time seawater $^{87}Sr/^{86}Sr$ values were between 0.7080 and 0.7085 (Halverson and Théou-Hubert, 2014)(Fig.16). Pennsylvanian marine sediments were deposited atop the ECCC during this time.

While these specific marine carbonates have not been analyzed, it would be a reasonable assumption that their Sr isotopic composition is ~0.7080. This assumption is based on Sr isotopic composition for other marine carbonates (Faure and Powell, 1972), and ocean waters during this time period with Sr isotopic compositions near 0.7080- 0.7085 (Halverson and Théou-Hubert, 2014) (Fig. 16).

The anomalous values from the ECCC are similar to those of the marine carbonates. It is possible groundwater circulating through the marine carbonates could have obtained radiogenic Sr and percolated down into the carbonatite, elevating the Sr isotopic compositions of the three anomalous values.

A low concentration of Sr in the groundwater would also allow the carbonatite to expel Sr into these fluids, causing the concentration of Sr in the carbonatite to decrease, as seen in the anomalous samples with concentrations of 40, 92, and 252 ppm. These concentrations are significantly lower than the rest of the samples, as seen in Table 7 and other Elk Creek core. For example, NioCorp hole NEC14-022 has an average Sr concentration of ~1806 ppm, containing multiple samples higher than 2000 ppm and two anomalously high samples of 25,930 and 17,100 ppm (NioCorp unpublished data, 2014).

Table 7 Strontium ratios and concentration from drill hole EC-001. Sample ID is the depth of the sample in feet. All data is from Brookins et al. (1975).

Sample ID	87Sr/86Sr	Sr (ppm)
905	.7039	1480
913	.7085	40
914	.7064	92
916	.7067	252
921.5	.7033	1020
929	.7040	1290
929.5 A	.7030	535
929.5 B	.7043	286
934.5	.7034	1750
936	.7055	1440
936.5	.7045	2940
938.5	.7051	2440
943 A	.7040	1670
943 B	.7056	685
944	.7048	1140
946	.7055	870
950	.7043	565
952	.7032	3500

Elevated Sr ratios have been cited in other carbonatites worldwide. Nikiforov et al. (2006) reported strontium ratios from carbonatites in Central Tuva. They were able to measure $^{87}Sr/^{86}Sr$ values from both altered and unaltered samples of whole rock carbonatite and primary and secondary minerals. A maximum ratio value of 0.70738 was measured from supergene calcite (Nikiforov et al., 2006). Their study determined that (1) the initial range of strontium isotopes for carbonatites is most likely 0.70416 to 0.70476 and (2) supergene alteration and addition of radiogenic strontium lead to a depletion of Sr in rock forming carbonates and thus an increase in the $^{87}Sr/^{86}Sr$ (Nikiforov et al., 2006).

7.4 Iron Oxide Alteration at Elk Creek

Iron oxide alteration is fairly abundant in the ECCC, and is observed in every rock type sampled in this research. Iron oxide alteration can range from trace to as high as 100% pervasive. Alteration minerals are limonite and hematite. The color of alteration ranges from yellow to very dark red. When altered pervasively the rock is typically very brittle and friable. Alteration typically occurs in fault and fracture zones and as thick veins. Rare earth element mineralization has been associated with hematite alteration in carbonatites worldwide (Andersen, 1987), including the ECCC (SRK Consulting, 2015).

It has been shown by several authors (Burberry et al. 2015; Carlson 1997; Marshak and Pulsen 1997), that southeastern Nebraska and northeastern Kansas have experienced multiple events of tectonic reactivation post Mississippian; including the NW-SE trending faults that offset the Nebraska segment of the MRS from the Kansas segment. The activation of NW-SE faults would allow oxidizing fluids to penetrate the carbonatite complex.

Drenth (2014) reported the possibility of faulting within the ECCC using aeromagnetic data, with a NW trend. The locations of the interpreted faults are shown in Fig. 10, indicated by a black dashed line. Drenth (2014) also noted that faulting could structurally control the magnetite-dolomite carbonatite and niobium mineralization since magnetite-dolomite carbonatite does not exist outside of that area (Fig. 11). Notably the B-B` transect is along Drenth's (2014) proposed fault

through the magnetite-dolomite carbonatite. Slickensides and/or gouge are recognized in alteration zones indicating movement within the carbonatite. In Fig. 18B, slickensides are visible along a fracture in the core where metallic hematite is present. Andersen (1984) noted that the alteration of the Fen Complex occurred in a zone of intense fracturing.

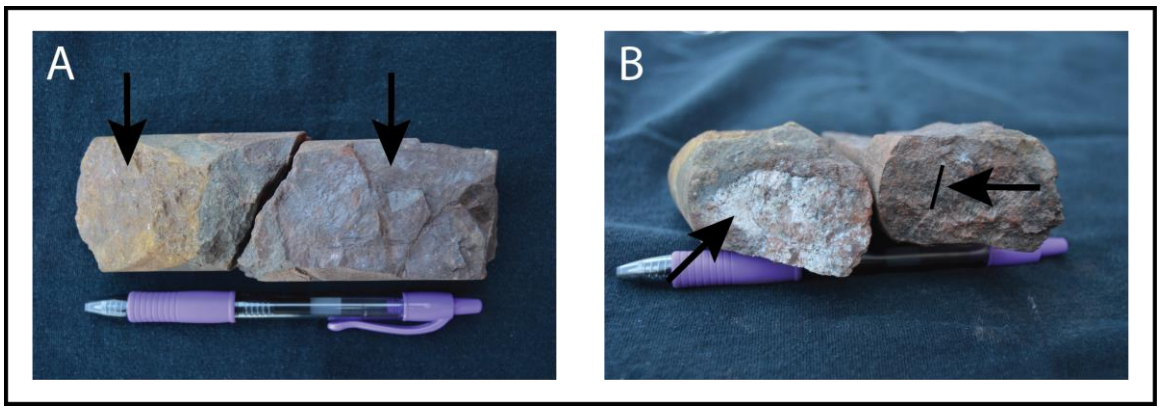

Fig. 18. Photo of altered core from drill hole EC-27. (A) Arrow on the left is pointing to limonite alteration and the arrow on the right to hematite alteration. (B) The arrow on the left is pointing to metallic hematite, and the arrow to the right is pointing to a traced slickenside on the fractured surface.

SRK Consulting also determined at least three major faults that bisect the carbonatite complex with a northeast trend (SRK Consulting, 2015). Five other tectonic related faults that cut through the carbonatite and Pennsylvanian carbonates were mentioned, with varying orientations (SRK Consulting, 2015).

Large iron oxide veins were documented in NioCorp Development's NI 43-101 report (SRK Consulting, 2015). SRK Consulting (2015), noted iron oxide veins that could be up to a meter thick. These veins are filled with the weakest material of any vein infill in the system; the material is characterized by friable altered

carbonatite rock with hematite alteration. Identifying and mapping the hematite alteration is necessary to isolate points of weakness in the carbonatite system when developing an underground mine. Figure 10 (profile B-B`) illustrates the depth and occurrence of hematite alteration within the zone of niobium mineralization.

Crosscutting relationships of hematite, limonite, and non-altered rocks within the system are examined to identify multiple events of alteration. Pictured below, Fig. 19 illustrates contact boundaries between alteration styles. In Fig. 19A the carbonatite has splotchy and locally pervasive hematite alteration surrounding dolomite grain boundaries, while the mafic dike has pervasive limonite alteration, with a sharp contact between the two alteration styles. This could be an indication of two different alteration events. However, it cannot be determined which came first.

It is not uncommon for several alteration events to occur in a single complex. Andersen (1987) determined there were two phases of alteration in the Fen Complex of south Norway: (1) occurred initially at oxygen fugacity below the hematite-magnetite (HM) buffer, ferrous iron and Mg were lost from the rock and (2) during a later stage when oxygen fugacity was above the HM buffer, and Fe was retained as hematite, while Mg and Ca were leached. Andersen (1987) also noted medium to heavy REE mineralization occurred in the highly hemititized rock, rødberg, in the Fen complex.

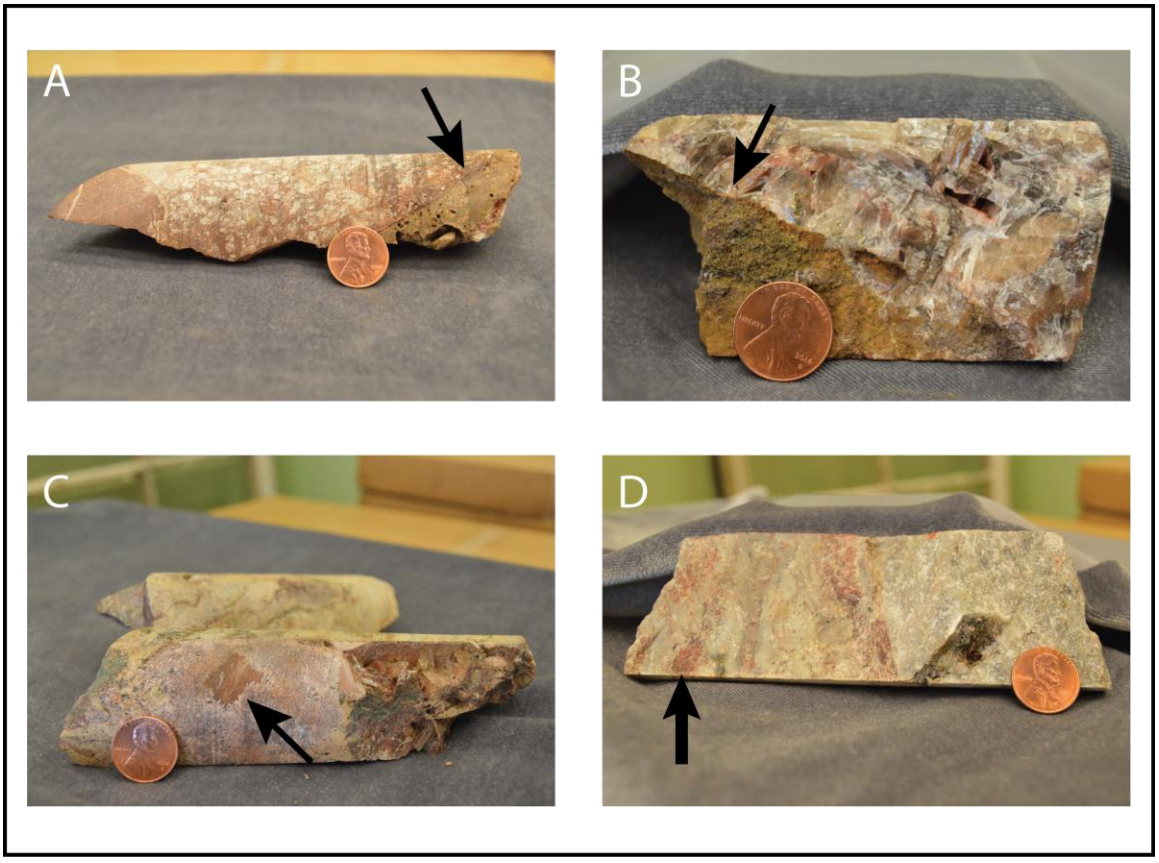

Fig. 19. Plate of alteration styles and contacts. (A) Dolomite carbonatite core cut by a mafic dyke with a sharp contact indicated by the arrow. The carbonatite has locally splotchy hematite alteration and hematite alteration surrounding grain boundaries. The mafic dyke has 100% pervasive limonite alteration (B) Sharp contact, indicated by the arrow, between 100% pervasive limonite alteration and crystalline barite (C) Crsytalline barite with hematite alteration, and what appears to be a hematite pseudomorph of pyrite, indicated by the arrow and (D) hematite alteration in barite-dolomite carbonatite, indicated by arrow.

It is important to identify and distinguish between the two (or more) alteration events to be able to trace REE mineralization in the ECCC. Molycorp logged significant REE mineralization in the barite-dolomite carbonatite that was heavily altered by hematite (SRK Consulting, 2015). The historic documents presented data percentages of LnO ranging from 2.13% to 2.75% in a 33 m long interval of core from hole EC-93 (SRK Consulting, 2015).

8. Conclusions

8.1 Sulfur Isotope Variations and Supergene Strontium

The $\delta^{34}S$ values reported in this thesis for the Elk Creek Carbonatite Complex are the first of their kind for this system. It is also the largest data set of sulfur isotopes for any individual carbonatite worldwide. In the ECCC the overall range of $\delta^{34}S$ values for sulfides is -10.85‰ to +2.31‰, and the range for sulfates is -11.89‰ to +16.67‰. There are several explanations for the wide variation in $\delta^{34}S$ values for both sulfate and sulfide: (1) Hypogene mineralization, (2) degassing, and (3) supergene alteration.

Hypogene mineralization in the ECCC is similar to that observed in carbonatites worldwide. $\delta^{34}S$ values for hypogene pyrite and barite range from -5.83‰ to -2.77‰ and +1.77‰ to +11.06‰, respectively. Using these values, an average formation temperature of 690°C was determined. A temperature of 690°C is in the range of early stage carbonatite evolution.

The $\delta^{34}S$ value for bulk sulfur in the system was also calculated from 3 different sulfide and sulfate mineral pairs. The calculations yielded a range for $\delta^{34}S_{\Sigma S}$ values of -2.23‰ to -1.64%, which is in the range of mantle sulfur. This is an indication that the sulfur in hypogene sulfur-bearing minerals came from a mantle source with local heterogeneities in ^{34}S concentration.

Evidence the ECCC underwent degassing was identified using three hypogene pyrite samples. These pyrite values were significantly more enriched in

^{34}S than the average ECCC sulfide minerals, with $\delta^{34}S$ values of +0.6‰, +2.26‰, and +2.31‰. The fluid that precipitated these minerals would have been enriched in ^{34}S, resulting from the outgassing of H_2S in an oxidizing environment.

The ECCC underwent supergene alteration, which significantly affected the $\delta^{34}S$ values of barite. The oxidation of pyrite at or near the surface of the carbonatite complex resulted in barite mineralization that was depleted in ^{34}S. The $\delta^{34}S$ values of the supergene sulfate range from -11.89‰ to -4.21‰.

Since the anomalously high $^{87}Sr/^{86}Sr$ values are too high to be considered mantle origin, and the carbonatite complex experienced intense weathering, it is not unlikely that the values are due to supergene alteration. With the strontium data available from Brookins et al. (1975), it appears as though the source of the high values is the Pennsylvanian marine sedimentary rocks that overlie the complex.

8.2 Iron Oxide Alteration

Iron oxide alteration is a prominent feature in the ECCC. The amount of alteration can range from trace amounts to 100% pervasive. The oxidized minerals are limonite and hematite.

There are multiple faults in the area with a NW-SE trend, including the one that offsets the Nebraska segment of the MRS from the Kansas segment. These fault and fracture zones structurally control the iron oxide alteration in the ECCC. Alteration profiles are a good tool to identify possible zones of weakness within the ECCC.

There is also evidence of at least two alteration events, as indicated by crosscutting relationships of hematite and limonite alteration. Identifying, distinguishing between alteration events, and mapping hematite alteration trends is a significant first step to tracing REE mineralization within the ECCC. The present findings lay the groundwork for unraveling the Elk Creek Carbonatite Complex's alteration history.

References

Anderson, R. R. (1997). Keweenawan Supergroup clastic rocks in the Midcontinent Rift of Iowa. *Geological Society of America Special Papers*, *312,* 211-230.

Andersen, T. (1987). A model for the evolution of hematite carbonatite, based on whole-rock major and trace element data from the Fen complex, southeast Norway. *Applied geochemistry*, *2*(2), 163-180.

Andersen, T. (1984). Secondary processes in carbonatites: petrology of "rødberg"(hematite-calcite-dolomite carbonatite) in the Fen central complex, Telemark (South Norway). *Lithos*, *17*, 227-245.

Ault, W. U., & Kulp, J. L. (1960). Sulfur isotopes and ore deposits. *Economic Geology*, *55*(1), 73-100.

Bickford, M. E., Harrower, K. L., Hoppe, W. J., Nelson, B. K., Nusbaum, R. L., & Thomas, J. J. (1981a). Rb-Sr and U-Pb geochronology and distribution of rock types in the Precambrian basement of Missouri and Kansas. *Geological Society of America Bulletin*, *92*(6), 323-341.

Bickford, M. E., Horrower, K. L., Hoppe, W. J., Nelson, B. K., Nusbaum, R. L., & Thomas, J. J. (1981b). Supplementary data for: Rb-Sr and U-Pb geochronology and distribution of rock types in the Precambrian basement of Missouri and Kansas. *Geological Society of America Bulletin*, *92*(6 Part II), 963-996.

Blessington, M. J. (2014). A Niobium Deposit Hosted by a Magnetite-Dolomite Carbonatite, Elk Creek Carbonatite Complex, Nebraska, USA.

Brookins, D. G., Treves, S. B., & Bolivar, S. L. (1975). Elk Creek, Nebraska, carbonatite: strontium geochemistry. *Earth and Planetary Science Letters*, *28*(1), 79-82.

Burberry, C. M., Joeckel, R. M., & Korus, J. T. (2015). Post-Mississippian tectonic evolution of the Nemaha Tectonic Zone and Midcontinent Rift System, SE Nebraska and N Kansas. *The Mountain Geologist*, *52*(4), 47-73

Burchett, R. R. (1980) Regional tectonics and seismicity of Eastern Nebraska, annual report July 1980-June 1981. *Paper in Natural Resources*, 580

Burke, W. H., Denison, R. E., Hetherington, E. A., Koepnick, R. B., Nelson, H. F., & Otto, J. B. (1982). Variation of seawater 87Sr/86Sr throughout Phanerozoic time. *Geology*, *10*(10), 516-519.

Cannon, W. F., & Hinze, W. J. (1992). Speculations on the origin of the North American Midcontinent rift. *Tectonophysics*, *213*(1), 49-55.

Carlson, M. P. (1997). Tectonic implications and influence of the Midcontinent Rift System in Nebraska and adjoining areas. *Geological Society of America Special Papers*, *312*, 231-234.

Carlson, M. P., and Treves, S. B. (2005) The Elk Creek Carbonatite, Southeast Nebraska- An Overview. *Natural Resources Research, 14*(1), 39-45

Chaussidon, M., Albarede, F., & Sheppard, S. M. F. (1987). Sulfur isotope heterogeneity in the mantle from ion microprobe measurements of sulfide inclusions in diamonds. *Nature*, *330*(6145), 242-244.

Chen, C., Liu, Y., Foley, S. F., Ducea, M. N., He, D., Hu, Z., ... & Zong, K. (2016). Paleo-Asian oceanic slab under the North China craton revealed by carbonatites derived from subducted limestones. *Geology*, *44*(12), 1039-1042.

Deines, P. (1989). Stable isotope variations in carbonatites. *Carbonatites: Genesis and Evolution. Unwin Hyman, London*, 301-359.

Dolton, G. L., & Finn, T. F. (1989). *Petroleum geology of the Nemaha Uplift, central mid-continent* (No. 88-450-D). Dept. of the Interior, US Geological Survey.

Drenth, B. J. (2014). Geophysical expression of a buried niobium and rare earth element deposit: The Elk Creek carbonatite, Nebraska, USA. *Interpretation*, *2*(4), SJ23-SJ33.

Drüppel, K., Wagner, T., & Boyce, A. J. (2006). Evolution of sulfide mineralization in ferrocarbonatite, Swartbooisdrif, Northwestern Namibia: constraints from mineral compositions and sulfur isotopes. *The Canadian Mineralogist*, *44*(4), 877-894.

Farmer, G. L., Kettler, R. M., & Verplanck, P. L. (2013). Geochemical and isotopic constraints on the age and origin of the Elk Creek carbonatite complex, SE Nebraska. In *GSA Rocky Mountain Section 65 th Annual Meeting, Paper* (pp. 21-7).

Farrell, S., Bell, K., & Clark, I. (2010). Sulfur isotopes in carbonatites and associated silicate rocks from the Superior Province, Canada. *Mineralogy and Petrology*, *98*(1-4), 209-226.

Faure, G., & Powell, J. L. (2012). *Strontium isotope geology* (Vol. 5). Springer Science & Business Media.

Field, C. W. (1966). Sulfur isotopic method for discriminating between sulfates of hypogene and supergene origin. *Economic Geology*, *61*(8), 1428-1435.

Gomide, C. S., Brod, J. A., Junqueira-Brod, T. C., Buhn, B. M., Santos, R. V., Barbosa, E. S. R., Cordeiro, P.F.O., Palmieri, M., Grasso, C.B., & Torres, M. G. (2013). Sulfur isotopes from Brazilian alkaline carbonatite complexes. *Chemical Geology*, *341*, 38-49.

Halverson, G. P., & Hubert-Théou, L. (2015). Seawater Sr Curve. *Encyclopedia of Scientific Dating Methods*, 733-739.

Heinrich, E. (1966). WM.,(1966) The geology of carbonatites. *Rand Monolly & Co., Chicago*.

Jensen, M. L., Ashley, R. P., & Albers, J. P. (1971). Primary and secondary sulfates at Goldfield, Nevada. *Economic Geology*, *66*(4), 618-626.

Joeckel, R., & Nicklen, B. (2007). Late Paleozoic weathering and residual accumulation of mineral on Elk Creek Carbonatite, Southeastern Nebraska, USA. In *2007 GSA Denver Annual Meeting*.

Johnson, J. W., Oelkers, E. H., & Helgeson, H. C. (1992). SUPCRT92: A software package for calculating the standard molal thermodynamic properties of minerals, gases, aqueous species, and reactions from 1 to 5000 bar and 0 to 1000 C. *Computers & Geosciences*, *18*(7), 899-947.

Lentz, D. R. (1999). Carbonatite genesis: a reexamination of the role of intrusion-related pneumatolytic skarn processes in limestone melting. *Geology*, *27*(4), 335-338.

Marini, L., Moretti, R., & Accornero, M. (2011). Sulfur isotopes in magmatic-hydrothermal systems, melts, and magmas. *Reviews in Mineralogy and Geochemistry*, *73*(1), 423-492.

Marshak, S., & Paulsen, T. (1997). Structural style, regional distribution, and seismic implications of midcontinent fault-and-fold zones, United States. *Seismological Research Letters*, *68*(4), 511-520.

Mitchell, R. H., & Krouse, H. R. (1975). Sulfur isotope geochemistry of carbonatites. *Geochimica et Cosmochimica Acta*, *39*(11), 1505-1513.

Mitchell, R. H., & Krouse, H. R. (1971). Isotopic Composition of Sulfur in Carbonatite at Mountain Pass, California. *Nature*, *231*(25), 182-182.

Miyoshi, T., Sakai, H., & Chiba, H. (1984). Experimental study of sulfur isotope fractionation factors between sulfate and sulfide in high temperature melts. *Geochemical Journal*, *18*(2), 75-84.

Morris, R.C. (1983). Supergene alteration of banded iron-formation. *Developments in Precambrian geology*, 6, 513-534

Nicholson, S. W., Shirey, S. B., Schulz, K. J., and Green, J. C. (1997) Rift-wide correlation of 1.1 Ga Midcontinent rift system basalts: implications for multiple mantle sources during rift development. *Canadian Journal of Earth Sciences, 34*, 504-520

Nicklen, B.L., and Joeckel, R.M.(2001, November). Preliminary report on some pre-late Pennsylvanian supra-basement weathering profiles in Southeastern Nebraska. In *GSA Annual Meeting, November 5-8, 2001,* 182.

Nikiforov, A. V., Bolonin, A. V., Pokrovsky, B. G., Sugorakova, A. M., Chugaev, A. V., & Lykhin, D. A. (2006). Isotope geochemistry (O, C, S, Sr) and Rb-Sr age of carbonatites in central Tuva. *Geology of Ore Deposits*, *48*(4), 256-276.

Nikiforov, A. V., Bolonin, A. V., Sugorakova, A. M., Popov, V. A., & Lykhin, D. A. (2005). Carbonatites of central Tuva: geological structure and mineral and chemical composition. *Geology of Ore Deposits C/C of Geologiia Rudnykh Mestorozhdenii*, *47*(4), 326.

Ohmoto, H. and Rye, R. (1979). Isotopes of sulfur and carbon. *Geochemistry of hydrothermal ore deposits*, 509-567.

Ohmoto, H. & Goldhaber M.(1997) Sulfur and carbon isotopes. *Geochemistry of Hydrothermal Ore Deposits. Barnes HL (Ed) J Wiley and Sons, New York*, 517-611.

Ojakangas, R. W., Morey, G. B., & Green, J. C. (2001). The Mesoproterozoic midcontinent rift system, Lake Superior region, USA. *Sedimentary Geology*, *141*, 421-442.

Planavsky, N. J., Bekker, A., Hofmann, A., Owens, J. D., & Lyons, T. W. (2012). Sulfur record of rising and falling marine oxygen and sulfate levels during the

Lomagundi event. *Proceedings of the National Academy of Sciences*, *109*(45), 18300-18305.

Ridley, J. (2013). *Ore deposit geology*. Cambridge University Press.

Rimstidt, J. D., & Vaughan, D. J. (2003). Pyrite oxidation: a state-of-the-art assessment of the reaction mechanism. *Geochimica et Cosmochimica Acta*, *67*(5), 873-880.

Rye, R. O., & Ohmoto, H. (1974). Sulfur and carbon isotopes and ore genesis: a review. *Economic Geology*, *69*(6), 826-842.

Seal, R. R. (2006). Sulfur isotope geochemistry of sulfide minerals. *Reviews in mineralogy and geochemistry*, *61*(1), 633-677.

Seal, R. R., Alpers, C. N., & Rye, R. O. (2000). Stable isotope systematics of sulfate minerals. *Reviews in Mineralogy and Geochemistry*, *40*(1), 541-602.

Sherer, R.W. (1978). Diamond Drill Log EC-15

SRK Consulting (2015). Amended NI 43-101 Technical Report Updated Preliminary Economic Assessment Elk Creek Niobium Project Nebraska. http://www.niocorp.com/images/ElkCreek_NI43-101_PEA-Updated_241900.030_026_20151016.pdf

Steeples, D. W., DuBois, S. M., & Wilson, F. W. (1979). Seismicity, faulting, and geophysical anomalies in Nemaha County, Kansas: Relationship to regional structures. *Geology*, *7*(3), 134-138.

Van Schmus, W. R., & Hinze, W. J. (1985). The midcontinent rift system. *Annual Review of Earth and Planetary Sciences*, *13*, 345.

Von Gehlen, K. (1967). S isotopes from the sulfide-bearing carbonatite of Phalaborwa, South Africa. *Trans Inst Min and Metall Sect B: Appl Earth Sci*, *76*(B), 223.

Wyllie, P.J. (1966). Experimental studies of carbonatite problems: the origin and differentiation of carbonatite magmas. *Carbonatites. Interscience Publishers, New York, 311-352*

Wyllie, P. J., & Tuttle, O. F. (1959). Synthetic carbonatite magma. *Nature*, *183*(4663), 770-770.

Xu, A. (1996). Mineralogy, petrology, geochemistry and origin of the Elk Creek carbonatite, Nebraska.

Yongfei, Z. (1990). Sulfur isotope fractionation in magmatic systems: models of Rayleigh distillation and selective flux. *Chinese Journal of Geochemistry*, *9*(1), 27-45.

Appendix A

Sample Location Rock Descriptions

UNL001: dolomite carbonatite; light-dark grey, fine- medium grain; trace magnetite, barite, trace fluorite, trace pyrite and chalcopyrite, hematite; localized flow banding with lamprophyre mixing

UNL002: dolomite carbonatite; light-dark grey, fine- medium grain; trace magnetite, barite, trace fluorite, trace pyrite and chalcopyrite, hematite; localized flow banding with lamprophyre mixing

UNL003: lamprophyre carbonatite breccia; olive green; medium- coarse grain; hematite, barite, chalcopyrite, trace magnetite clasts, dolomite phenocrysts

UNL004: dolomite carbonatite; light grey; very fine grain; dolomite, chalcopyrite, barite, hematite; hematite alteration 100% pervasive on 3 quarters of the fracture including the vug samples were retrieved; possible barite- dolomite carbonatite cross cutting the dolomite carbonatite surrounding sample are

UNL005: mafic; pale olive green; very fine- coarse grain; dolomite, barite, chalcopyrite; minimal limonite- hematite alteration

UNL006: carbonate- bearing lamprophyre breccia; light olive grey- green; very fine-coarse grain; dolomite, apatite, chalcopyrite, barite, hematite, biotite, magnetite

UNL007: carbonate- bearing lamprophyre breccia; light olive grey- green; very fine-coarse grain; dolomite, apatite, chalcopyrite, barite, hematite, biotite, magnetite

UNL008: carbonate- bearing lamprophyre breccia; light olive grey- green; very fine-coarse grain; dolomite, apatite, chalcopyrite, barite, hematite, biotite, magnetite

UNL009: magnetite- dolomite carbonatite massive; yellow- brownish (highly altered, can not tell original color); very fine grain- locally coarse grain; magnetite, barite, chalcopyrite, hematite, limonite, calcite (veins)

UNL010: magnetite- dolomite carbonatite massive; yellow- brownish (highly altered, can not tell original color); very fine grain- locally coarse grain; magnetite, barite, chalcopyrite, hematite, limonite, calcite (veins)

UNL011: dolomite carbonatite; light grey; very fine- fine grain; abundant fluorite, abundant barite, trace chalcopyrite

UNL012: magnetite- dolomite carbonatite massive; light grey; very fine to fine

grain; barite, magnetite, chalcopyrite, fluorite

UNL013: magnetite- dolomite carbonatite breccia; light to dark grey; coarse grain; barite, magnetite, chalcopyrite, disseminated pyrite, hematite

UNL014: magnetite- dolomite carbonatite breccia; light grey; coarse grain; magnetite, pyrite, hematite, chalcopyrite; hematite alteration and local lamprophyre carbonatite mixing

UNL015: magnetite- dolomite carbonatite breccia; light grey; coarse grain; magnetite, pyrite, hematite, chalcopyrite; hematite alteration and local lamprophyre carbonatite mixing

UNL016: carbonate- bearing lamprophyre veinleted; dark olive green; very fine-medium grain; dolomite, biotite, trace magnetite, dolomite, hematite, barite, chalcopyrite

UNL017: carbonate- bearing lamprophyre breccia; yellow-brown; coarse grain; dolomite, barite, chalcopyrite, magnetite, hematite, trace fluorite; highly altered

UNL018: dolomite carbonatite; original color overprinted with brick red alteration; very fine- fine grain; hematite, barite, chalcopyrite

UNL019: dolomite carbonatite massive; light grey; very fine- fine grain; barite, chalcopyrite, trace hematite; highly altered by hematite and limonite

UNL020: magnetite- dolomite carbonatite breccia; yellow- brown due to alteration; coarse grain; barite, fluorite carbothermal vein, trace chalcopyrite, hematite; highly altered by limonite

UNL021: magnetite- dolomite carbonatite breccia; light- medium grey; coarse grain; magnetite, hematite, barite, chalcopyrite

UNL022: magnetite- dolomite carbonatite breccia; light- medium grey; coarse grain; magnetite, hematite, barite, chalcopyrite

NEC001- NEC004: magnetite- dolomite carbonatite breccia; light grey; coarse grain; magnetite, barite, pyrite, fluorite, trace hematite

NEC005-NEC008: magnetite- dolomite carbonatite; original color overprinted with yellow-brown limonite alteration; very fine- medium grain; locally brecciated; barite, chalcopyrite, hematite, magnetite, trace fluorite

EC27_001- EC27_001_03: dolomite carbonatite breccia; light grey- cream, coarse grain, chalcopyrite, fluorite, apatite, barite; lamprophyre clasts

EC27_002- EC27_005: magnetite bearing lamprophyre breccia; green- grey; coarse grain; magnetite, dolomite, hematite, barite, biotite; alteration varying between samples from 20-100% pervasive, red-brown hematite alteration and yellow limonite alteration

EC28_001_02: magnetite- dolomite carbonatite breccia; dark grey; coarse grain; hematite, magnetite, barite, fluorite, trace chalcopyrite; locally foliated; local pervasive alteration of limonite 80-100%

EC28_002- EC28_003_03: magnetite- dolomite carbonatite breccia; dark grey; coarse grain; magnetite, hematite, barite, fluorite, trace chalcopyrite

Appendix B

Sulfur-Bearing Mineral Chemical Formulas

Mineral	Mineral Formula
Sulfide:	
Pyrite	FeS_2
Chalcopyrite	$CuFeS_2$
Galena	PbS
Arsenopyrite	$FeAsS$
Pyrrhotite	$Fe_{1-x}S$
Pentlandite	$(Fe,Ni)_9S_8$
Bornite	Cu_5FeS_4
Cubanite	$CuFe_2S_3$
Marcasite	FeS_2
Millerite	NiS
Molybdenite	MoS_2
Sphalerite	$(Zn,Fe)S$
Sulfate:	
Barite	$BaSO_4$
Gypsum	$CaSO_4$
Jarosite	$KFe_3(SO_4)_2(OH)_6$

Appendix C

Sample ID and Drill Hole

Sample ID	Box Number
UNL001	EC-15
UNL002	EC-15
UNL003	EC-15
UNL004	EC-12
UNL005	EC-30
UNL006	EC-15
UNL007	EC-15
UNL008	EC-15
UNL009	EC-18
UNL010	EC-18
UNL011	EC-48
UNL012	EC-48
UNL013	EC-48
UNL014	EC-15
UNL015	EC-15
UNL016	EC-21
UNL017	EC-04
UNL018	EC-76
UNL019	EC-48
UNL020	EC-86
UNL021	EC-32
UNL022	EC-32
NEC001	NEC14-013
NEC002	NEC14-013
NEC003	NEC14-013
NEC004	NEC14-013
NEC005	NEC14-012
NEC006	NEC14-012
NEC007	NEC14-012
NEC008	NEC14-012
EC27_001	EC-27
EC27_001_2	EC-27
EC27_001_3	EC-27
EC27_002	EC-27
EC27_003	EC-27
EC27_003_2	EC-27
EC27_004	EC-27
EC27_005	EC-27
EC27_006	EC-27
EC28_001_2	EC-28
EC28_002	EC-28
EC28_003	EC-28
EC28_003_2	EC-28
EC28_003_3	EC-28

Sample Drill Hole Location Map